

Synthetic Designs and Structural Investigations of Biomimetic Ni–Fe Thiolates

Debashis Basu, T. Spencer Bailey, Noémie Lalaoui,^{1b} Casseday P. Richers, Toby J. Woods,^{1b} and Thomas B. Rauchfuss^{*1b}

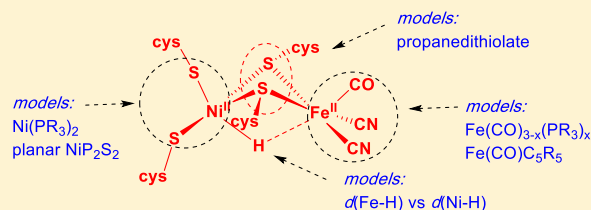
School of Chemical Sciences, University of Illinois, Urbana, Illinois 61801, United States

Federica Arrigoni and Giuseppe Zampella

Department of Biotechnology and Biosciences, University of Milano-Bicocca, Piazza della Scienza 2 20126 Milan, Italy

Supporting Information

ABSTRACT: Described are the syntheses of several Ni(μ -SR)₂Fe complexes, including hydride derivatives, in a search for improved models for the active site of [NiFe]-hydrogenases. The nickel(II) precursors include (i) nickel with tripodal ligands: Ni(PS₃)[−] and Ni(NS₃)[−] (PS₃^{3−} = tris(phenyl-2-thiolato)phosphine, NS₃^{3−} = tris(benzyl-2-thiolato)amine), (ii) traditional diphosphine-dithiolates, including chiral diphosphine *R,R*-DIPAMP, (iii) cationic Ni(phosphine-imine/amine) complexes, and (iv) organonickel precursors Ni(*o*-tolyl)Cl(tmeda) and Ni(C₆F₅)₂. The following new nickel precursor complexes were characterized: PPh₄[Ni(NS₃)] and the dimeric imino/amino-phosphine complexes [NiCl₂(PCH=N^{An})₂] and [NiCl₂(PCH₂NH^{An})₂] (P = Ph₂PC₆H₄-2-). The iron(II) reagents include [Cp*Fe(CO)₂(thf)]BF₄, [Cp*Fe(CO)(MeCN)₂]BF₄, Fe₂(CO)₄, FeCl₂(diphos)(CO)₂, and Fe(pdt)(CO)₂(diphos) (diphos = chelating diphosphines). Reactions of the nickel and iron complexes gave the following new Ni–Fe compounds: Cp*Fe(CO)Ni(NS₃), [Cp(CO)Fe(μ -pdt)Ni(dppbz)]BF₄, [(*R,R*-DIPAMP)Ni(μ -pdt)(H)Fe(CO)₃]BAR^F₄, [(PCH=N^{An})Ni(μ -pdt)(Cl)Fe(dppbz)(CO)]BF₄, [(PCH₂NH^{An})Ni(μ -pdt)(Cl)Fe(dppbz)(CO)]BF₄, [(PCH=N^{An})Ni(μ -pdt)(H)Fe(dppbz)(CO)]BF₄, [(dppv)(CO)Fe(μ -pdt)]₂Ni, {H[(dppv)(CO)Fe(μ -pdt)]₂Ni}BF₄, and (C₆F₅)₂Ni(μ -pdt)Fe(CO)₂(dppv) (DIPAMP = (CH₂P(C₆H₄-2-OMe)₂)₂; BAR^F₄[−] = [B(C₆H₃-3,5-(CF₃)₂)₄][−]). Within the context of Ni-(SR)₂-Fe complexes, these new complexes feature new microenvironments for the nickel center: tetrahedral Ni, chirality, imine, and amine coligands, and Ni–C bonds. In the case of {H[(dppv)(CO)Fe(μ -pdt)]₂Ni}⁺, four low-energy isomers are separated by ≤ 3 kcal/mol, one of which features a biomimetic HNi(SR)₄ site, as supported by density functional theory calculations.



INTRODUCTION

[NiFe] hydrogenases are enzymes that catalyze the reversible oxidation of H₂, a process that is relevant to the metabolism of many microorganisms.¹ Motivated by the implications of H₂ redox and related reactions,² much effort has been expended on replicating the active site of these enzymes.³ Progress in modeling the active site can be measured by the structural similarity of models and the various catalytically significant states. These states include Ni–SI, Ni–R, Ni–L, and Ni–C. Structural models for the first three states have been described, although they lack biomimetic terminal ligands. Analysis of models for the Ni(II)–Fe(II)-hydride state, Ni–R, is presented in Figure 1. The figure highlights aspects where synthetic models are deficient or differ strongly from the natural system.

From the synthetic perspective, models either manipulate the Ni site or the Fe site. In this report we continue this approach, emphasizing expanding the range of ligands on nickel. We address, sometimes with only incremental progress, the following deficiencies in modeling: (1) nonplanar Ni(II)

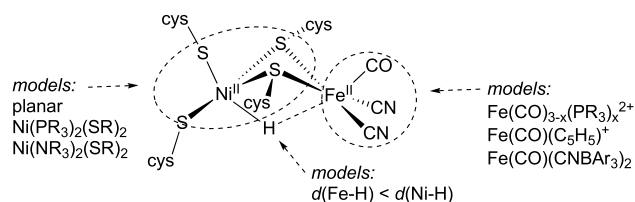


Figure 1. Active site of [NiFe]-hydrogenase core in the Ni–R state.

sites, (2) the rarity of Ni(SR)_x sites ($x > 2$), (3) the asymmetry of the Ni···H–Fe interactions, and (4) the introduction of exchangeable terminal ligand sites on Ni, specifically those based on Ni–C sigma bonds.

Problems 1 and 2: Nonplanar Ni(II) sites and nonbridging NiSR sites. The Ni-center in the Ni–SI_a is a distorted tetrahedron with four cysteine-thiolate ligands, two terminal

Received: October 22, 2018

and two bridging. The terminal thiolates are implicated as bases in proton transfer reactions,^{4,5} such as the heterolysis of H₂. In the two models with terminal Ni-SR centers, the corresponding hydride derivatives could not be prepared.^{6,7} All Ni(II)-containing models feature square planar or five-coordinate Ni. Thus, one goal in this work focused on incorporating Ni centers with a rigidly nonplanar coordination sphere and at least one terminal thiolate.

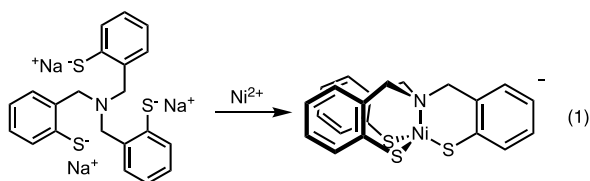
Problem 3: the Asymmetry of the Ni...H-Fe Interactions. Several hydride-containing NiFe complexes are known.³ They are all of the type L₂Ni(SR)₂FeHL₃. In these models the Fe-H bond is usually⁸ shorter than the Ni-H bond,⁹⁻¹² whereas in the enzyme, the $d_{\text{Ni-H}} < d_{\text{Fe-H}}$.¹³ The shorter Ni-H distance underscores the role of Ni as the hydride carrier, whereas the Fe center serves as a redox-inactive Lewis acid. In this paper, the Ni coordination sphere is manipulated in an effort to strengthen the Ni-H interaction.

RESULTS AND DISCUSSION

1. Ni(II) Complexes of Tripodal PS₃ and NS₃ Ligand and Their [NiFe] Derivatives. Nonplanar Ni(II) thiolate complexes were targeted several years ago by Liaw, Koch and Millar, and their co-workers.¹⁴⁻¹⁹ They described several complexes of tripodal phosphine trithiolates^{20,21} (Figure S1), but not the corresponding Ni-Fe derivatives. Our efforts initially focused on the phosphine trithiolates, but quickly turned to amine trithiolates.

Ni(PS₃)- and Ni(NS₃)-Based Models. Using P(C₆H₄-2-SH)₃, Liaw, Millar, and their co-workers described promising nickel precursors with terminal thiolates. Our experiments showed however that in its reactions with iron reagents, [Ni(PS₃H)-PPh₃]¹⁶ (Scheme S1, Figures S2-S11) serves as a source of PPh₃ or transfers the PS₃³⁻ chelate to Fe. One solution to the transfer of the PPh₃ involves use of [Ni(PS₃)]⁻, but this species does not exist per se.

In view of the challenges with the Ni(PS₃)-based models, we turned to complexes derived from N(CH₂C₆H₄-2-SH)₃, (abbreviated N(SH)₃). This tripodal ligand was developed by Koch et al., who characterized the tetrahedral complexes [M(NS₃)]⁻ (M = Ga(III), Zn(II), Fe(II)).²²⁻²⁴ Considerable progress has also been reported on the synthesis of N(SH)₃.^{25,26} As shown schematically in eq 1, the NS₃ ligand



envelops the metal center because it features six-membered chelate rings. In contrast the PS₃³⁻ ligands, forming only five-membered chelate rings, leave one site open for coordination of a fifth ligand.²⁰

The complex [Ni(NS₃)]⁻ was synthesized by combining [N(SNa)₃] with NiCl₂·6H₂O in ethanol solution (eq 1).

The salt PPh₄[Ni(NS₃)] was isolated as green crystals. The solid is soluble in polar organic solvents to give air-stable solutions that are intensely green owing to strong absorptions at 477 ($\epsilon = 3800$) and 637 nm ($\epsilon = 1200 \text{ cm}^{-1} \text{ M}^{-1}$, Figure S12), consistent with tetrahedral Ni(II). This salt was characterized by X-ray crystallography, ESI-MS, ¹H NMR spectroscopy, and elemental analyses. Its ¹H NMR spectrum in

CD₂Cl₂ solution spanned from $\delta 300$ to -20 (Figure S13), consistent with the paramagnetic nature of this complex. ESI-MS in negative mode displayed the molecular ion peak (Figure S14).

According to X-ray crystallography, PPh₄[Ni(NS₃)] consists of a pseudotetrahedral Ni complex (Figure 2). The S-Ni-S

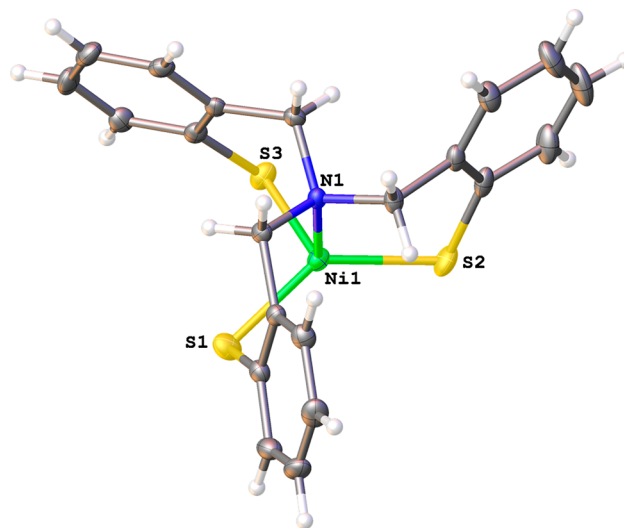


Figure 2. ORTEP diagram (50% probability) of the anion in PPh₄[Ni(NS₃)]. Ni(1)–N(1), 2.0310(15) Å; Ni(1)–S(1), 2.2621(5) Å; Ni(1)–S(3), 2.2705(5) Å; Ni(1)–S(2), 2.2829(5) Å. Selected angles: N(1)–Ni(1)–S(1): 100.49(4)°; N(1)–Ni(1)–S(3), 101.02(4)°; N(1)–Ni(1)–S(2), 100.83(4)°; S(1)–Ni(1)–S(3), 105.03(2)°; S(1)–Ni(1)–S(2), 136.60(2)°; S(3)–Ni(1)–S(2), 107.36(2)°.

bond angles range from 105 to 136°, perhaps due to the Jahn–Teller distortion arising from the $(e_2)^4(t_2)^4$ configuration. A related [Ga(NS₃)] complex exhibits average S–Ga–S and N–Ga–S angles of 115 and 102°, respectively.²² The Ni–N bond length is ~ 2.03 Å, whereas the Ni–S bond-lengths range from ~ 2.26 – 2.28 Å. Solutions of Ph₄P[Ni(NS₃)] are unreactive toward CO and PPh₃. In contrast, adducts of the type [Ni(PS₃)CO]⁻ have been characterized crystallographically.²⁰

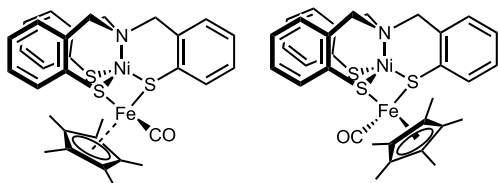
To generate Fe–Ni complexes, reactions of [Ni(NS₃)]⁻ with cyclopentadienyl iron complexes were investigated.^{27,28}

Treatment of Na[Ni(NS₃)] or PPh₄[Ni(NS₃)] with [CpFe(CO)₂(thf)]BF₄ gave an immediate reaction. The deep brown product exhibited a pair of ν_{CO} bands, shifted by 25–30 cm⁻¹ to lower energy with respect to the cationic precursor (Figure S15). This initial product is assigned as the 1:1 adduct Ni(NS₃)Fe(CO)₂Cp. Allowing solutions of this adduct to stand in ambient light, the pair of ν_{CO} bands is replaced by a new broad peak at 1952 cm⁻¹. Similar shifts are observed for other L_xNi(SR)₂Fe(CO)Cp complexes.²⁶ The positive-ion ESI-mass spectrum of the decarbonylated product (despite its being charge-neutral) shows an intense peak envelope centered at $m/z = 1173.9$, which corresponds to [Ni(NS₃)-Fe(CO)Cp]₂ (Figure S16). The same product was obtained from the reaction of [Ni(NS₃)]⁻ with [CpFe(CO)(MeCN)₂]-BF₄ ($\nu_{\text{CO}} = 2013 \text{ cm}^{-1}$, Figures S17–S19). The experimental peak envelope was well simulated with theoretical values. The ¹H NMR spectrum of the product was broad.

Experiments were also conducted on related Cp*Fe(CO)-based complexes (Cp* = C₅Me₅). Being bulky, the Cp*Fe-based reagent was expected to favor formation of a 1:1 Ni–Fe

derivative.²⁹ Indeed, treating a CH_2Cl_2 solution of $[\text{Ni}(\text{NS}_3)]^-$ salts with $[\text{Cp}^*\text{Fe}(\text{CO})(\text{MeCN})_2]\text{BF}_4$ generated a new complex with a single ν_{CO} band shifted to lower energy vs the cationic iron precursor (Figure S20). On the basis of the relative positions of CO and Cp^* ligands, two stereoisomers are possible (Scheme 1), as have been observed for other

Scheme 1. Structures Proposed for Isomers of $[\text{Ni}(\text{NS}_3)\text{Fe}(\text{CO})\text{Cp}^*]$



$\text{Ni}(\mu\text{-SR})_2\text{Fe}(\text{CO})\text{Cp}^*$ complexes.^{30,31} The positive-ESI-mass spectrum shows intense peaks corresponding to M^+ and $[\text{M-CO}]^+$ (Figure S21). The isotopic distributions for both peak envelopes match simulated spectra (Figures S22 and S23).

2. $\text{Ni}(\text{P}_2\text{S}_2) + \text{Fe}(\text{II})$ Reagents. The addition of electrophilic iron reagents to nickel-(diphos)-dithiolates is a traditional route to $\text{Ni}(\text{SR})_2\text{-Fe}$ complexes (diphos = chelating diphosphine ligand).^{3,27} Analogous methods using planar NiN_2S_2 complexes have been well investigated, where $\text{N}_2\text{S}_2^{2-}$ is a tetradentate diaminedithiolate.^{32,33} Relative to NiN_2S_2 , $\text{Ni}(\text{dithiolate})(\text{diphos})$ complexes are advantageous because the geometry at Ni is less restrained, which allows the generation of tetrahedral Ni(I) derivatives.³

$[\text{Cp}(\text{CO})\text{Fe}(\mu\text{-pdt})\text{Ni}(\text{diphosphine})]^+$. Reinvestigation of Schroeder's synthesis of $[\text{Cp}(\text{CO})\text{Fe}(\text{pdt})\text{Ni}(\text{dppe})]^+$,³⁴ although mainly confirmatory, is briefly described because the stepwise refinement of methodology is instructive. According to Schroeder, the reaction of $\text{Ni}(\text{pdt})(\text{dppe})$ and $\text{CpFe}(\text{CO})_2\text{I}$ gives $[\text{Cp}(\text{CO})\text{Fe}(\mu\text{-pdt})\text{Ni}(\text{dppe})]^+$ as well as a considerable amount of $[\text{Ni}_2(\mu\text{-pdt})(\mu\text{-I})(\text{dppe})_2]^+$. The salt $[\text{CpFe}(\text{CO})_2(\text{thf})]\text{BF}_4$ was found to react with $\text{Ni}(\text{pdt})(\text{dppe})$ in a less complicated manner (Scheme 2, Figures S26–S27). As revealed by in situ ^{31}P NMR spectroscopy, however, $[\text{Ni}_2(\mu\text{-pdt})(\mu\text{-Cl})(\text{dppe})_2]^+$ was a significant byproduct. When performed in THF (Figure S28), the reaction produced $[\text{CpFe}(\text{CO})(\text{dppe})]^+$ as a side product. The lability of the diphosphine was suppressed by replacing $\text{Ni}(\text{pdt})(\text{dppe})$ with $\text{Ni}(\text{pdt})(\text{dppv})$ ($\text{dppv} = \text{cis-1,2-C}_2\text{H}_2(\text{PPh}_2)_2$, Figure S29–S32). With this optimized protocol, the reaction $\text{Ni}(\text{pdt})(\text{dppv}) + [\text{CpFe}(\text{CO})_2(\text{thf})]^+$ was found to produce a previously undetected intermediate. With two equally intense ^{31}P NMR signals, this new species is assigned as $[\text{Cp}(\text{CO})_2\text{Fe}(\mu\text{-pdt})\text{Ni}(\text{dppv})]^+$, wherein only one thiolate bridges Ni and Fe.²⁰ The related reaction $\text{Ni}(\text{pdt})(\text{dppbz}) + [\text{CpFe}(\text{CO})(\text{NCMe})_2]^+$ produced high yields of $[\text{Cp}(\text{CO})\text{Fe}(\mu\text{-$

$\text{pdt})\text{Ni}(\text{dppbz})]^+$, which was characterized by X-ray crystallography as its BF_4^- salt (Figures 3, S33–S35).

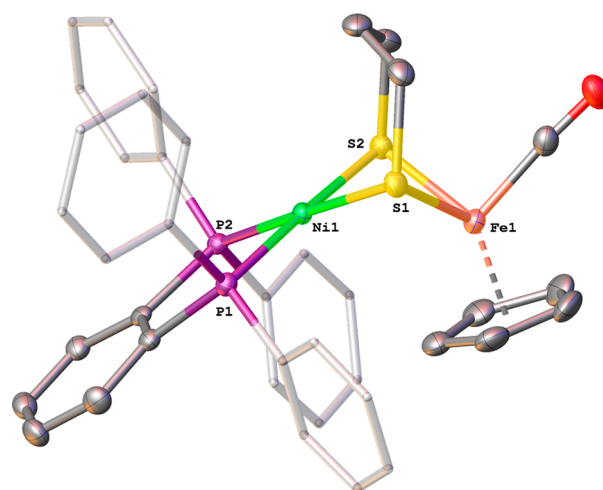
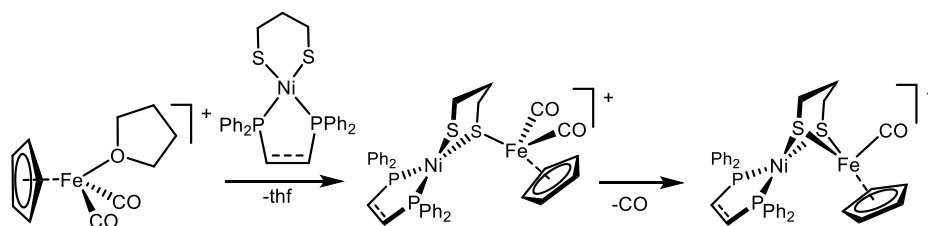


Figure 3. ORTEP diagram (50% probability) of the cation in the salt $[\text{Cp}(\text{CO})\text{Fe}(\mu\text{-pdt})\text{Ni}(\text{dppbz})]\text{BF}_4$ (H atoms were removed for clarity). Selected distances (Å): Ni(1)–P(2), 2.1508(7); Ni(1)–P(1), 2.1577(7); Ni(1)–S(2), 2.2104(7); Ni(1)–S(1), 2.2221(7); Ni(1)–Fe(1), 2.8066(5); Fe(1)–S(1), 2.2852(9); Fe(1)–S(2), 2.2784(7) Å.

$[(\text{CO})_3\text{Fe}(\text{H})(\mu\text{-pdt})\text{Ni}(\text{R,R-DIPAMP})]^+$. Another route from Ni(dithiolate)(diphos) to $\text{Ni}(\text{SR})_2\text{-Fe}$ complexes involves use of $\text{FeI}_2(\text{CO})_4$ as a source of $[\text{Fe}(\text{CO})_3]^+$.¹⁰ This approach was adopted to prepare a complex containing R,R-DIPAMP ($\text{DIPAMP} = 1,2\text{-bis}[(2\text{-methoxyphenyl})(\text{phenyl})\text{phosphino}]\text{-ethane}$). In addition to being chiral, R,R-DIPAMP features 2-methoxyphenyl groups, which are suitably positioned to coordinate³⁵ to nickel, although this aspect was not manifested. As summarized in Scheme 3, $\text{NiCl}_2(\text{R,R-DIPAMP})$ was converted to $\text{Ni}(\text{pdt})(\text{R,R-DIPAMP})$.³¹ ^{31}P and ^1H NMR spectra confirm the diamagnetic nature of the complex (Figures S36–S37). Treatment of $\text{Ni}(\text{pdt})(\text{R,R-DIPAMP})$ with $\text{FeI}_2(\text{CO})_4$ yielded the corresponding iodo-bridged $[\text{NiFe}]$ complex $[(\text{R,R-DIPAMP})\text{Ni}(\mu\text{-pdt})(\mu\text{-I})\text{Fe}(\text{CO})_3]^+$, which was characterized in situ by FT-IR spectrum. Reduction of this cationic iodo complex with Cp_2Co generated $(\text{R,R-DIPAMP})\text{Ni}(\mu\text{-pdt})\text{Fe}(\text{CO})_3$, which was also characterized in situ by its FT-IR spectrum. Reaction of this reduced species with $\text{H}(\text{OEt}_2)_2\text{BAR}_4^{\text{F}}$ gave $[(\text{R,R-DIPAMP})\text{Ni}(\mu\text{-pdt})(\text{H})\text{Fe}(\text{CO})_3]\text{BAR}_4^{\text{F}}$, which was fully characterized ($\text{BAR}_4^{\text{F}-} = [\text{B}(\text{C}_6\text{H}_3-3,5\text{-}(\text{CF}_3)_2)_4]^-$, Scheme 3, Figures S36–S41). The pattern of the ν_{CO} bands in the FT-IR spectrum product and the intermediates (Figure 4, Figures S38–S39) match those observed for related (achiral) complexes.¹⁰

Scheme 2. Reaction of $\text{Ni}(\text{pdt})(\text{diphos})$ and $[\text{CpFe}(\text{CO})_2(\text{thf})]^+$



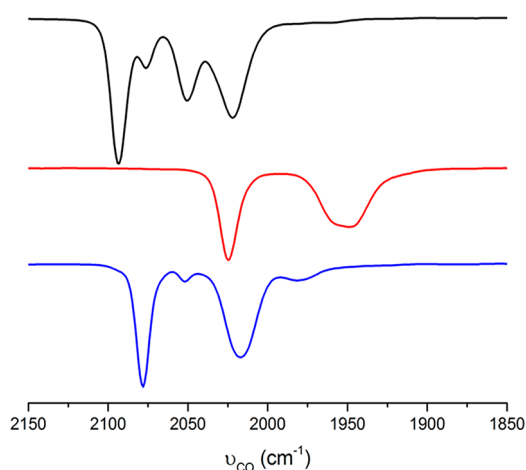
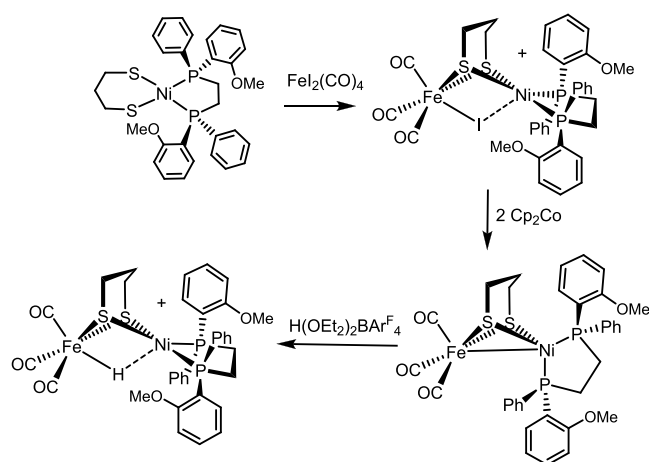
Scheme 3. Synthesis of $[(R,R\text{-DIPAMP})\text{Ni}(\mu\text{-pdt})(\text{H})\text{Fe}(\text{CO})_3]^+$


Figure 4. IR spectra (CH_2Cl_2) of $[(R,R\text{-DIPAMP})\text{Ni}(\mu\text{-pdt})(\text{I})\text{Fe}(\text{CO})_3]\text{I}$ (top), $[(R,R\text{-DIPAMP})\text{Ni}(\mu\text{-pdt})\text{Fe}(\text{CO})_3]$ (middle), and $[(R,R\text{-DIPAMP})\text{Ni}(\mu\text{-pdt})(\text{H})\text{Fe}(\text{CO})_3]\text{BARF}_4$ (bottom).

The crystallographically determined structure of $[(R,R\text{-DIPAMP})\text{Ni}(\mu\text{-pdt})(\text{H})\text{Fe}(\text{CO})_3]\text{BARF}_4$ is shown in Figure 5. The Ni–Fe distance is 2.65 Å. The Ni and Fe centers adopt square-pyramidal and pseudo-octahedral geometries, respectively. The Ni–H and Fe–H distances are 1.94(4) and 1.58(4) Å, respectively. ^{31}P NMR spectrum of $[(R,R\text{-DIPAMP})\text{Ni}(\mu\text{-pdt})(\text{H})\text{Fe}(\text{CO})_3]\text{BARF}_4$ exhibited two slightly broad peaks ($\delta_{65.0}$, 70.2), indicating the P's on Ni are nonequivalent as required by the presence of the chiral diphosphine (Figures S40–S41).

3. $\text{NiCl}_2(\text{N-chelate}) + \text{Fe}(\text{pdt})(\text{CO})_2(\text{diphosphine})$. An established route to nickel–iron dithiolates involves the reaction $\text{NiCl}_2\text{L}_2 + \text{Fe}(\text{pdt})(\text{CO})_2\text{L}'_2$. This method is useful when the corresponding $\text{Ni}(\text{SR})_2\text{L}_2$ building block is not available, as illustrated by Song's synthesis of models containing $\text{Ni}(\text{dppp})^{2+}$ centers ($\text{dppp} = \text{Ph}_2\text{PCH}_2\text{CH}_2\text{CH}_2\text{PPh}_2$).³⁶ We applied this approach to the preparation of Ni–Fe complexes with Ni(phosphine-amine/imine) centers. The majority of Ni–Fe–H complexes are derived from nickel diphosphine centers.³ Since NiCl_2 derivatives of P–N ligands tend to be pentacoordinate,³⁷ Ni(PN)-based models were anticipated to adopt novel structures.

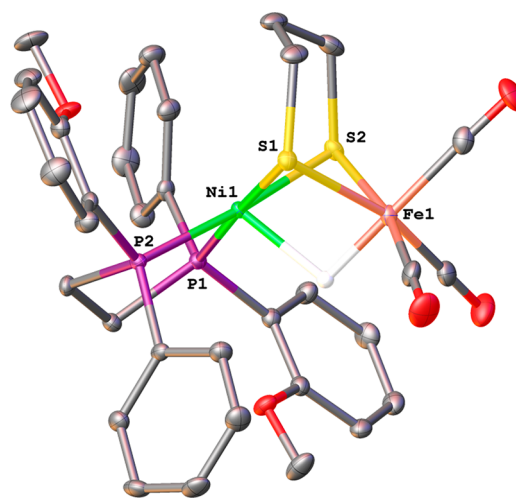


Figure 5. ORTEP diagram (50% probability) of $[(R,R\text{-DIPAMP})\text{Ni}(\mu\text{-pdt})(\text{H})\text{Fe}(\text{CO})_3]\text{BARF}_4$ (H atoms were removed for clarity). Selected distances (Å): Ni(1)–H(1): 1.94(4); Fe(1)–H(1): 1.58(4); Ni(1)–Fe(1): 2.6589(5); Ni(1)–S(1): 2.2153(8); Ni(1)–S(2): 2.2174(9); Ni(1)–P(1): 2.1629(8); Ni(1)–P(2): 2.1669(9); Fe(1)–S(1): 2.3119(9); Fe(1)–S(2): 2.3136(8).

$[\text{Ni}(\text{P-imine})]$ -Based Models. This effort focused on complexes of the imine-phosphine $\text{PCH}=\text{N}^{\text{An}}$ derived from 2-diphenylphosphinobenzaldehyde and anisidine ($\text{H}_2\text{NC}_6\text{H}_4\text{OMe}$).³⁸ The reaction of equimolar $\text{NiCl}_2(\text{DME})$ and $\text{PCH}=\text{N}^{\text{An}}$ gave a yellow paramagnetic 1:1 complex ($\text{DME} = 1,2\text{-dimethoxyethane}$). As shown by X-ray crystallography, the complex is the dimer $[\text{NiCl}_2(\text{PCH}=\text{N}^{\text{An}})]_2$ (Figure 6). It features a pair of pentacoordinate Ni centers with two bridging chloride ligands. This dimeric motif is well-precedented in other $[\text{NiCl}_2(\text{P-N})]_2$ complexes.^{39–41} The five-coordinated paramagnetic high-spin nickel(II) centers adopt pseudo-square pyramidal geometry ($\tau = 0.26$ ⁴²) with apical phosphines.

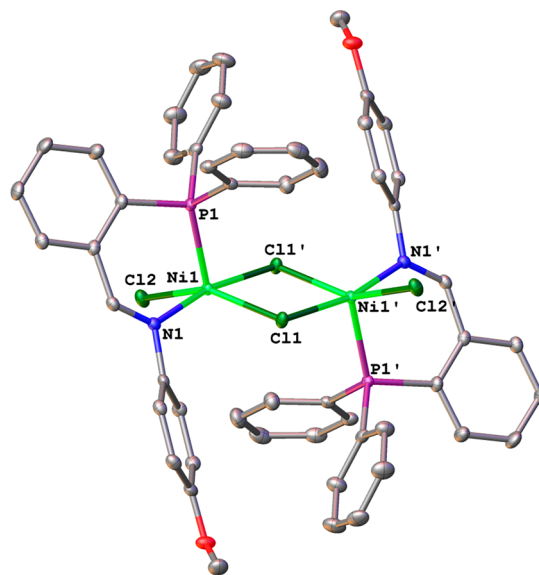
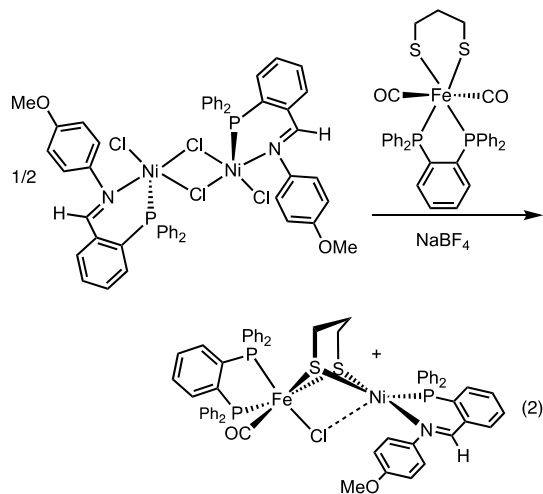


Figure 6. ORTEP diagram (50% probability) of $[\text{NiCl}_2(\text{PCH}=\text{N}^{\text{An}})]_2$; H atoms were removed for clarity. Selected distances (Å): Ni(1)–Cl(1): 2.3638(5); Ni(1)–Cl(2): 2.3128(5); Ni(1)–Cl(1): 2.4033(6); Ni(1)–P(1): 2.2842(3); Ni(1)–N(1): 2.074(1).

The targeted $\text{Ni}(\text{SR})_2\text{Fe}$ complex was prepared by combining $\text{Fe}(\text{pdt})(\text{CO})_2(\text{dppbz})$ and $[\text{NiCl}_2(\text{PCH}=\text{N}^{\text{An}})]_2$. When conducted in acetone solution at 0°C in the presence of NaBF_4 , the reaction gave $[(\text{PCH}=\text{N}^{\text{An}})\text{Ni}(\mu\text{-pdt})\text{ClFe}(\text{dppbz})(\text{CO})]\text{BF}_4$ as the exclusive product (eq 2). With ν_{CO}

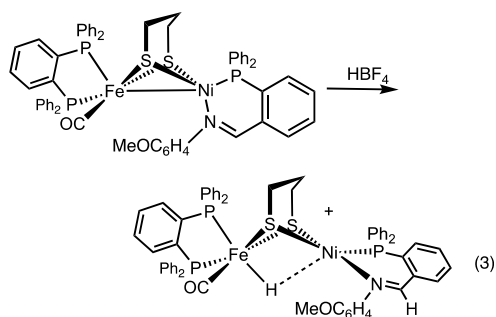


= 1946 cm^{-1} (Figure S42), the cation resembles related complexes such as $[(\text{dppe})\text{Ni}(\mu\text{-pdt})\text{ClFe}(\text{dppb})\text{CO}]^+$.⁴³ The (+)-ESI-mass spectrum displayed peak envelopes for both the molecular ion ($[\text{M}]^+$) and $[\text{M}-\text{CO}]^+$ (Figure S43).

The ^{31}P NMR spectrum exhibits three doublets (Figure S44). Signals at $\delta 67.7$ and 72.6 are assigned to the FeP centers, and that at $\delta 19.4$ is assigned to the NiP centers. Three nonequivalent phosphine sites indicates that the diphosphine on Fe is apical-basal, as is observed in other complexes of the type $[(\text{diphos})\text{Ni}(\mu\text{-pdt})\text{ClFe}(\text{diphos})(\text{CO})]^+$.⁸ The ^1H NMR spectrum is well resolved (Figure S45).

The reduced complex $(\text{PCH}=\text{N}^{\text{An}})\text{Ni}(\mu\text{-pdt})\text{Fe}(\text{dppbz})\text{CO}$ was obtained by treating $[(\text{PCH}=\text{N}^{\text{An}})\text{Ni}(\mu\text{-pdt})\text{ClFe}(\text{dppbz})(\text{CO})]\text{BF}_4$ with Cp^*Co . Yellow solids that precipitated from the reaction solution are presumed to be salts of $[\text{Cp}^*\text{Co}]^+$. The targeted $(\text{PCH}=\text{N}^{\text{An}})\text{Ni}(\mu\text{-pdt})\text{Fe}(\text{dppbz})\text{CO}$ was isolated as a brown solid, which is soluble in THF, toluene, and CH_2Cl_2 . In the IR spectrum of this $[\text{Ni}^{\text{I}}\text{Fe}^{\text{I}}]$ derivative, ν_{CO} appears at 1919 cm^{-1} vs 1946 cm^{-1} for $[(\text{PCH}=\text{N}^{\text{An}})\text{Ni}(\mu\text{-pdt})\text{ClFe}(\text{dppbz})(\text{CO})]\text{BF}_4$ (Figure S46). The ^{31}P NMR spectrum revealed three new sets of peaks, indicating that the diphosphine on Fe is apical-basal (Figure S47).

Protonation of $(\text{PCH}=\text{N}^{\text{An}})\text{Ni}(\mu\text{-pdt})\text{Fe}(\text{dppbz})\text{CO}$ with $\text{HBF}_4\cdot\text{Et}_2\text{O}$ yielded the corresponding hydride. This product is characterized by a ν_{CO} band at 1945 cm^{-1} (Figure



S49), which is shifted by 26 cm^{-1} vs its precursor (eq 3). The ^{31}P NMR spectrum consisted of two sets of three equi-intensity peaks, indicating the presence of two species (Figure S50). ESI-MS in the positive mode displayed peak envelopes for both the molecular ion ($[\text{M}]^+$) and $[\text{M}-\text{CO}]^+$ for $[(\text{PCH}=\text{N}^{\text{An}})\text{Ni}(\text{pdt})(\text{H})\text{Fe}(\text{dppbz})(\text{CO})]^+$ (Figures S52–S53). The ^1H NMR spectrum revealed one hydride peak (triplet) at δ -0.7 (Figure S54). Although the complex is stable in the solid state, the hydride signal disappears over a period of days in CD_2Cl_2 solution. We tentatively assigned the product as $[(\text{PCH}=\text{N}^{\text{An}})\text{Ni}(\mu\text{-pdt})(\text{H})\text{Fe}(\text{dppbz})(\text{CO})]\text{BF}_4$, whereas the two sets of peaks in ^{31}P NMR can be attributed to (i) the hydride complex ($\delta 26.8, 91.21, 94.6$), and (ii) the decomposition product ($\delta 19.8, 72.9, 75.8$) in CH_2Cl_2 .

[Ni(P-amine)]-Based Models. Using a method completely analogous to the preceding section, Ni–Fe complexes were pursued with *amino*-phosphines. The required nickel amino-phosphine precursor was prepared from the phosphine-amine chelate $\text{PCH}_2\text{NH}^{\text{An}}$, which in turn was obtained by borohydride reduction of $\text{PCH}=\text{N}^{\text{An}}$ (Figures S55–S56). Treating $\text{PCH}_2\text{NH}^{\text{An}}$ with $\text{NiCl}_2(\text{DME})$ gave $[\text{NiCl}_2(\text{PCH}_2\text{NH}^{\text{An}})]_2$, isolated in analytical purity as a yellow paramagnetic solid. X-ray crystallography established that the complex is dimeric, consisting of a pair of pentacoordinate Ni centers with bridging chloride ligands (Figure 7).²⁴ The five-coordinated nickel(II) centers adopt pseudo square pyramidal geometry ($\tau = 0.13$ – 0.17).

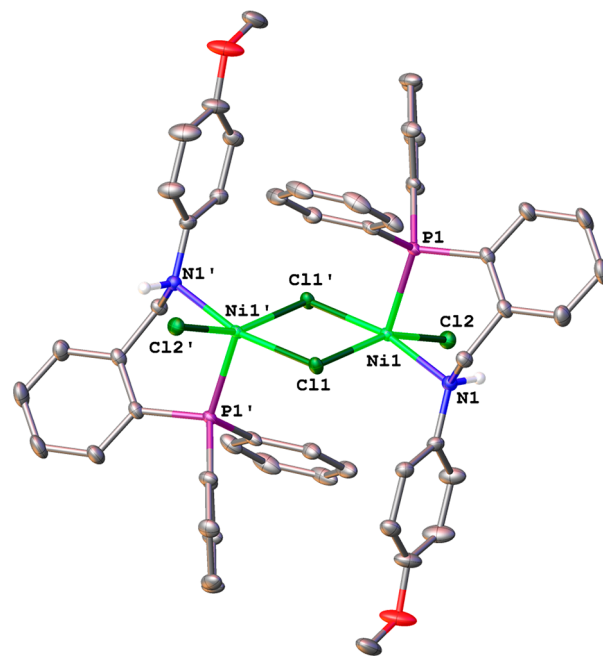
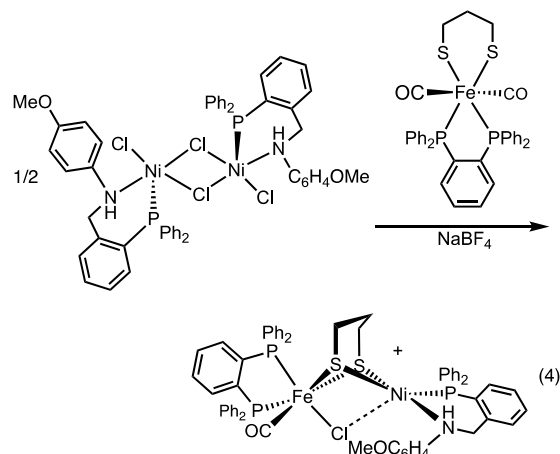


Figure 7. ORTEP diagram (50% probability) of $[\text{NiCl}_2(\text{PCH}_2\text{NH}^{\text{An}})]_2$. H atoms were removed for clarity except N-H. Selected distances (Å): Ni(1)–N(1), 2.1173(11); Ni(1)–Cl(2), 2.3065(3); Ni(1)–P(1), 2.3271(4); Ni(1)–Cl(1), 2.3544(3); Ni(1)–Cl(1)′, 2.3584(3).

The preparation of the amine-supported Ni–Fe complex followed the method for the aforementioned $(\text{PCH}=\text{N}^{\text{An}})\text{Ni}$ –Fe complex. Combining $\text{Fe}(\text{pdt})(\text{CO})_2(\text{dppbz})$ and $[\text{NiCl}_2(\text{PCH}_2\text{NH}^{\text{An}})]_2$ in acetone in the presence of NaBF_4 gave $[(\text{PCH}_2\text{NH}^{\text{An}})\text{Ni}(\mu\text{-pdt})\text{ClFe}(\text{dppbz})(\text{CO})]\text{BF}_4$ in excellent yield (eq 4). The (+)-ESI-mass spectrum displayed

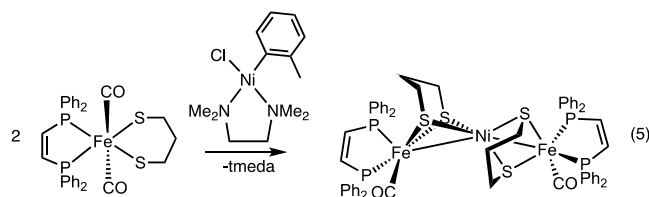


peak envelopes for both the molecular ion ($[M]^+$) and $[M-CO]^+$ (Figure S57). Judging from its IR spectrum ($\nu_{CO} = 1949 \text{ cm}^{-1}$), the cation resembles the analogous $PCH=N^{An}$ complex (Figure S58). The ^{31}P NMR spectrum revealed a single species (three peaks), showing that the secondary amine coordinates diastereoselectively (Figure S59).

Attempted reduction of $[(PCH_2NH^{An})Ni(\mu\text{-pdt})ClFe(dppbz)(CO)]BF_4$ with Cp^*_2Co produced $[Cp^*_2Co]^+$ as well as a large amount of free PCH_2NH^{An} , as verified respectively by ^1H and ^{31}P NMR spectroscopy (Figure S61). The formation of free phosphine indicates that the PCH_2NH^{An} does not stabilize the reduced complex. Attempted dehydrohalogenation of $[(PCH_2NH^{An})Ni(\mu\text{-pdt})ClFe(dppbz)(CO)]^+$ using $NaOMe$ also yielded a large amount of free PCH_2NH^{An} (Figure S62).

4. $NiR_2 + Fe(pdt)(CO)_2(\text{diphosphine})$. The modeling of the active site would be facilitated if it were possible to introduce ligands at nickel *after* formation of the $Ni(\mu\text{-SR})_2Fe$ or $Ni(\mu\text{-SR})_2(\mu\text{-H})Fe$ core. One specific idea was that terminal thiolates could be introduced by protonolysis of Ni-carbon sigma bonds using thiols.^{44,45} $Ni(\text{-SR})_2\text{-Fe}$ complexes with Ni-carbon sigma-bonds are however unknown. To simplify the synthetic chemistry, we chose to focus on nickel aryl complexes.

$Ni(\text{tolyl})Cl(\text{tmeda}) + Fe(pdt)(CO)_2(\text{diphos})$. Experiments aimed at generating Ni-aryl substituents entailed reaction of $Fe(pdt)(CO)_2(\text{dppv})$ and $NiCl(2\text{-tolyl})(\text{tmeda})$ ($\text{tmeda} = \text{tetramethylethylenediamine}$).^{46,47} With a labile diamine ligand, this Ni complex was expected to serve as a source of $Ni(C_6H_4\text{-}2\text{-Me})Cl$. In practice, the reaction proved more complicated. Chromatographic workup reliably gave yields of $\sim 30\%$ of $[(\text{dppv})(CO)Fe(\mu\text{-pdt})]_2Ni$, isolated as a chocolate brown, air-stable solid (eq 5).



This complex is one of several with the $Fe(SR)_2Ni(SR)_2Fe$ core.^{27,48} The distinctive aspect of our $Fe(SR)_2Ni(SR)_2Fe$ complex is that the constituent metals are not all divalent. The metal centers have a collective formal charge of 4+. The tetrahedral geometry of the Ni center is appropriate for Ni(0)

or Ni(I), leading to descriptions of the complex as $Fe(1.5)\text{-}Ni(1)Fe(1.5)$ or $Fe(II)Ni(0)Fe(II)$. The $Fe(1.5)Ni(1)Fe(1.5)$ description is favored because the ν_{CO} band at 1914 cm^{-1} is within 3 cm^{-1} of that for $(\text{dppv})(CO)Fe(\mu\text{-pdt})Ni(\text{dppv})$, which we had previously assigned as $Fe(I)\text{-}Ni(I)$.⁸ The formation of a reduced complex is consistent with $NiCl(2\text{-tolyl})(\text{tmeda})$ functioning as a source of Ni(0) via ligand redistribution and reductive elimination of bitolyl.⁴⁷ The complex undergoes reversible oxidation at -1.2 V .

The complex $[(\text{dppv})(CO)Fe(\mu\text{-pdt})]_2Ni$ is C_2 -symmetric, consisting of a central $[Ni(pdt)_2]^{2n-}$ center attached to a pair of $[(\text{dppv})(CO)Fe]^{n+}$ modules (Figure 8). The S-Ni-S

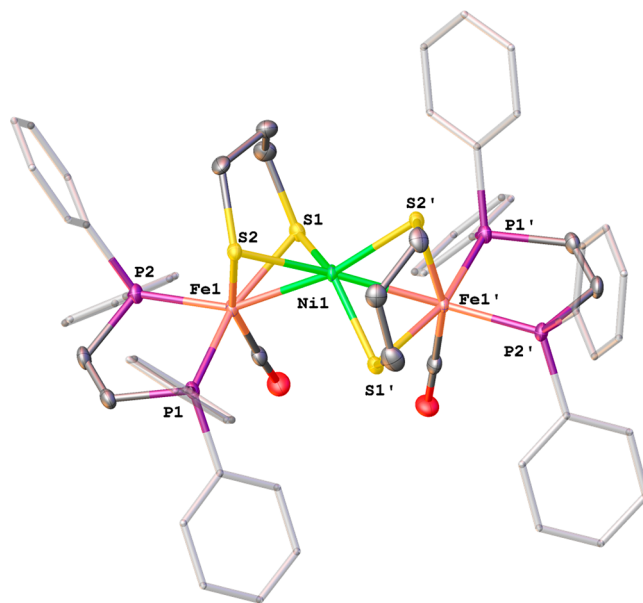


Figure 8. ORTEP diagram (50% probability) of $[(\text{dppv})(CO)Fe(\mu\text{-pdt})]_2Ni$. H atoms were removed for clarity. Selected distances (\AA) [DFT-calculated values]: Fe(1)–Ni(1), 2.4532(3) [2.523]; Fe(1)–P(1), 2.2134(7); Fe(1)–P(2), 2.1871(6); Fe(1)–S(1), 2.2589(6) [2.314]; Fe(1)–S(2), 2.2925(7) [2.271]; Ni(1)–S(1), 2.2459 [2.290]; Ni(1)–S(2), 2.2612 [2.235].

angles range from 88 to 138° , with an average of 114° . The two Fe centers are equivalent, as imposed by the crystallographic site symmetry. Counting Ni–Fe bond as a sixth ligand, the Fe centers are pseudo-octahedral, which is also consistent with the S–Fe–P and P–Fe–C angles. The dppv ligands span apical and basal coordination site on Fe, which is typical for $Fe(I)Ni(I)$ derivatives such as $(\text{dppv})(CO)Fe(\mu\text{-pdt})Ni(\text{dppv})$.⁸

The ^{31}P NMR spectrum $[(\text{dppv})(CO)Fe(\mu\text{-pdt})]_2Ni$ features two broad singlets, assigned to phosphorus centers attached to apical and basal sites on each Fe as observed also for $(\text{dppv})(CO)Fe(\mu\text{-pdt})Ni(\text{dppv})$.⁸ Upon warming the sample to 80°C , the two ^{31}P NMR singlets broadened into the baseline, but coalescence was not observed.

The crystallographic structure of $[(\text{dppv})(CO)Fe(\mu\text{-pdt})]_2Ni$ matches the low-energy density functional theory (DFT) result, although the computed bond distances are about 5% longer than those observed experimentally. The stereochemistry of the $(\text{dppv})(CO)Fe(pdt)NiL_2$ core for the low energy structures follow structural patterns for related NiFe complexes:⁸ lower energy isomers differ with respect to apical-basal dppv vs basal-basal dppv (6.7 kcal/mol). A structure

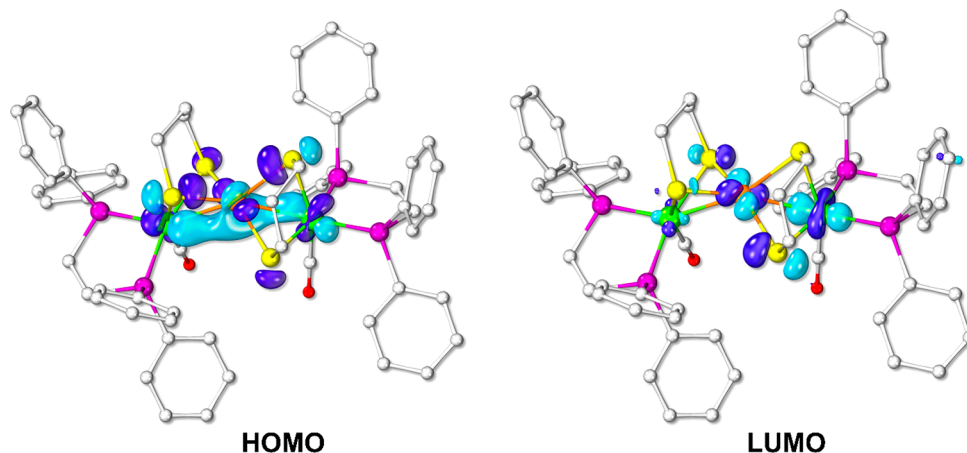


Figure 9. Frontier MOs of $[(\text{dppv})(\text{CO})\text{Fe}(\mu\text{-pdt})]_2\text{Ni}$ (isosurface cutoff = 0.05 a.u.).

with planar NiS_4 center is observed only at 12.7 kcal/mol. This planar nickel structure can also be described with a dihedral angle (θ) of 0° between the S1-Ni1-S2 and S1'-Ni1-S2' planes. High spin (triplet) states are high in energy, especially for larger values of θ . Attempts to antiferromagnetically localize spins on metal centers (through the Broken Symmetry approximation) failed. NBO charges on Fe1, Ni, and Fe2 are -0.20 , $+0.61$, and -0.20 , respectively in 1A and -0.18 , $+0.53$, and -0.18 in 1B. In other words, Fe centers carry more negative charge than Ni independent of θ . The frontier molecular orbitals are localized almost entirely on metal and sulfur centers. The HOMO is predominantly Fe1–Ni1–Fe2 σ bonding, whereas the LUMO is Fe1–Ni1 and Ni1–Fe2 σ^* antibonding (Figure 9).

With oxidation states assigned as $\text{Fe}(1.5)\text{Ni}(1)\text{Fe}(1.5)$ or $\text{Fe}(\text{I})\text{Ni}(\text{II})\text{Fe}(\text{I})$, $[(\text{dppv})(\text{CO})\text{Fe}(\mu\text{-pdt})]_2\text{Ni}$ has two reducing equivalents and may therefore be expected to protonate. Indeed, as a CH_2Cl_2 solution, the complex reacts with HBF_4 to give the dark purple cation $[\text{H}[(\text{dppv})(\text{CO})\text{Fe}(\mu\text{-pdt})]_2\text{Ni}]^+$ (eq 6). This hydride complex was initially identified by its ESI-

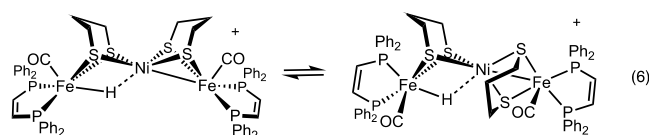


Figure 10. ORTEP diagram (50% probability) of the cation in $[\text{H}[(\text{dppv})(\text{CO})\text{Fe}(\mu\text{-pdt})]_2\text{Ni}]^+\text{BF}_4^-$. H atoms were removed for clarity. Selected distances (\AA): Fe(1)–Ni(1), 2.5327(9) [2.572]; Fe(2)–Ni(1), 2.5653(9) [2.598]; Fe(2)–H, 1.65(4) [1.635]; Ni(1)–H, 1.82(4) [1.745]; Fe(2)–S(3), 2.285(1) [2.264]; Fe(2)–S(4), 2.274(1) [2.262]; Ni(1)–S(1), 2.197(1) [2.249]; Ni(1)–S(2), 2.203(1) [2.248]; Ni(1)–S(3), 2.223(1) [2.263]; Ni(1)–S(4), 2.217(1) [2.264].

MS spectrum. The new species features ν_{CO} bands at 1943 and 1961 cm^{-1} in CH_2Cl_2 solution assigned to unprotonated and protonated FeCO centers, respectively.

The structure of $[\text{H}[(\text{dppv})(\text{CO})\text{Fe}(\mu\text{-pdt})]_2\text{Ni}]^+\text{BF}_4^-$ was elucidated by single crystal X-ray diffraction (Figure 10). The connectivity in $[(\text{dppv})(\text{CO})\text{Fe}(\mu\text{-pdt})]_2\text{Ni}$ is retained; however protonation induces Ni to convert from tetrahedral to square planar geometry.⁴⁹ The Fe–H and Ni–H distances are 1.65(4) and 1.82(4) \AA , respectively. Such unsymmetrically bridging hydrides are typical for other Ni–Fe hydrides.⁹ The HFe–Ni distance is only slightly elongated (2.5653(9) \AA) compared with the neighboring unprotonated Ni–Fe fragment (2.5327(9) \AA). The Fe(1)–P and Fe(2)–P distances are almost the same, but the Fe–S distances for unprotonated Fe are 0.05 \AA shorter than the ~ 2.28 \AA HFe–S distances.

According to ^1H NMR spectra, solutions of $[\text{H}[(\text{dppv})(\text{CO})\text{Fe}(\mu\text{-pdt})]_2\text{Ni}]^+$ exist as a mixture of three isomers as revealed by three sets of signals in the hydride region (Figure 11). These signals are centered at $\delta -4.9$ (t, $J(\text{H},\text{P}) = 36$ Hz),

-6.6 (broad), and -15.5 (s) with respective integrated intensities of 1:1.5:2.5 at room temperature. The broad signal at $\delta -6.6$ sharpens to a singlet at elevated temperatures. The ^{31}P NMR spectrum of $[\text{H}[(\text{dppv})(\text{CO})\text{Fe}(\mu\text{-pdt})]_2\text{Ni}]^+\text{BF}_4^-$ consists of five peaks, which can be assigned to the three isomeric hydrides (Figure S64). The relative intensities of the ^1H and ^{31}P NMR signals are mutually consistent. In addition to $[\text{H}[(\text{dppv})(\text{CO})\text{Fe}(\mu\text{-pdt})]_2\text{Ni}]^+\text{BF}_4^-$, the salt $[\text{H}[(\text{dppv})(\text{CO})\text{Fe}(\mu\text{-pdt})]_2\text{Ni}]^+\text{BAR}_4^-$ was also prepared. The change in counteranion did not noticeably affect the NMR results, indicating that the isomer distribution is unaffected by ion pairing.

Additional insight into the structures of and relationships between the isomeric hydrides was provided by low temperature NMR studies (Figure S65). Solutions prepared by dissolving crystals of $[\text{H}[(\text{dppv})(\text{CO})\text{Fe}(\mu\text{-pdt})]_2\text{Ni}]^+\text{BF}_4^-$ in CD_2Cl_2 at -80°C contain exclusively the isomer with a hydride signal at $\delta -4.9$. At -80°C , the ^{31}P NMR spectrum consists of four equally intense signals, which are decoalesced daughters of the $\delta 86$ and 72 signals observed in the thermally equilibrated room temperature spectrum. The relative

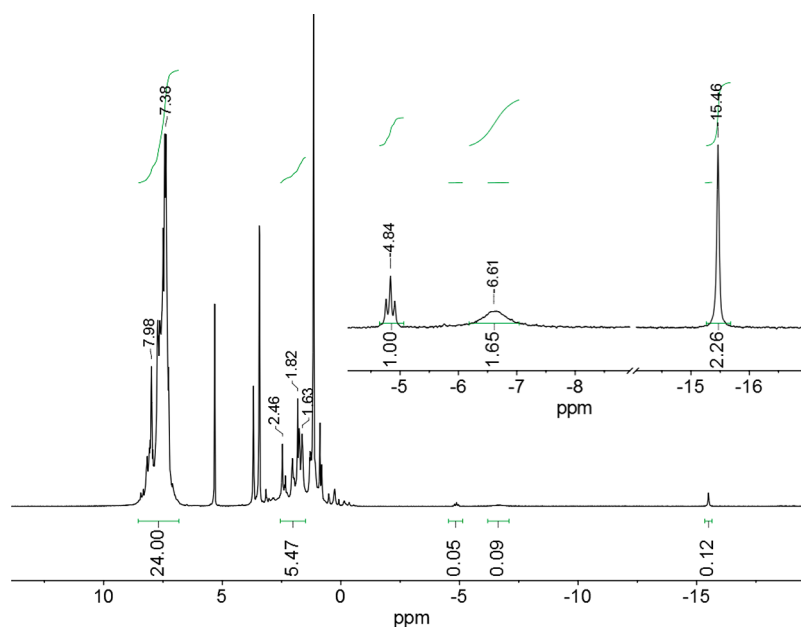


Figure 11. ^1H NMR spectra of $\{\text{H}[(\text{dppv})(\text{CO})\text{Fe}(\mu\text{-pdt})]_2\text{Ni}\}^+\text{BF}_4^-$ (CD_2Cl_2 solution) providing evidence for three isomers.

frequencies of these four signals indicate that the splitting does not arise from spin–spin coupling; instead, these signals are assigned to four nonequivalent phosphine sites. Because the cation $\{\text{H}[(\text{dppv})(\text{CO})\text{Fe}(\mu\text{-pdt})]_2\text{Ni}\}^+$ is C_s -symmetric, the observation of four signals may be attributed to frozen conformations of the pdt^{2-} backbones. Upon warming the solution to $-45\text{ }^\circ\text{C}$, the four ^{31}P NMR signals coalesce into two broad singlets, which continue to sharpen as the solution is warmed to room temperature. These two singlets are assigned to protonated and unprotonated $\text{Fe}(\text{dppv})(\text{CO})$ sites. These data provide some insight into the slowness of the degenerate hydride (or proton) transfer between two equivalent FeNi sites. Also appearing in the $-45\text{ }^\circ\text{C}$ spectrum are three signals in intensity 1:1:2 (the latter intensity from accidental degeneracy), assigned to second isomer. Near room temperature these three signals coalesce into the singlet at δ 86.8, indicating again that two $\text{Fe}(\text{dppv})$ sites are equilibrating rapidly on the NMR time scale. At $-15\text{ }^\circ\text{C}$ two broad singlets appear at low field, assigned to a third isomer. These signals appear concomitant with the appearance of the hydride signal at $-\delta$ 15.5.

Like other $\text{Ni}(\text{SR})_2\text{Fe}$ hydrides, $\{\text{H}[(\text{dppv})(\text{CO})\text{Fe}(\mu\text{-pdt})]_2\text{Ni}\}^+$ is an active catalyst for hydrogen evolution from chloroacetic acid, as demonstrated by cyclic voltammetry (Figures S67–S68).

The crystallographic structure for $\{\text{H}[(\text{dppv})(\text{CO})\text{Fe}(\mu\text{-pdt})]_2\text{Ni}\}^+$ matches the low-energy DFT result. The DFT structure is one of four isomers that are separated by ≤ 3 kcal/mol. These isomeric hydrides differ in terms of the stereochemistry of the $\text{Fe}(\text{dppv})(\text{CO})$ site and θ , the dihedral or “twist” angle defined by the S1NiS2 and S3NiS4 planes. All stable isomers feature bridging hydrides. The two lowest-energy isomers are depicted in eq 6 and Figure 12.

The DFT-calculated chemical shifts of the hydride ligand, δ_{H} , correlate with the twist angle. When $\theta = 0$, $\sim\delta_{\text{H}}-2$ (e.g., in $[\text{IA}]^+$) vs the observed chemical shift of δ -4.9. For the isomers with $\theta \approx 60^\circ$, δ_{H} ranges from $\sim\delta$ -9.1 to -10.2.

$\text{Ni}(\text{C}_6\text{F}_5)_2(\text{dioxane})_2 + \text{Fe}(\text{pdt})(\text{CO})_2(\text{diphos})$. The previous experiment using $\text{NiCl}(2\text{-tolyl})(\text{tmeda})$ failed to deliver Ni–Fe

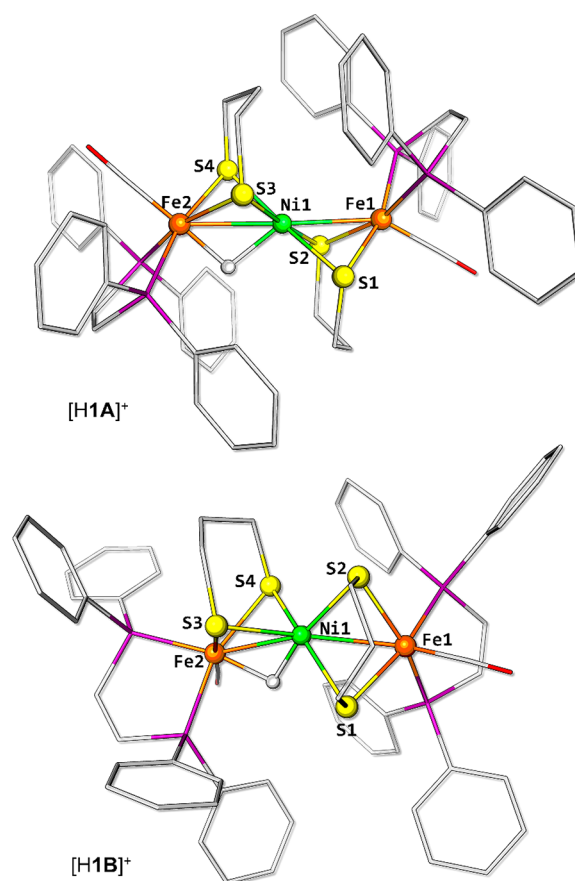
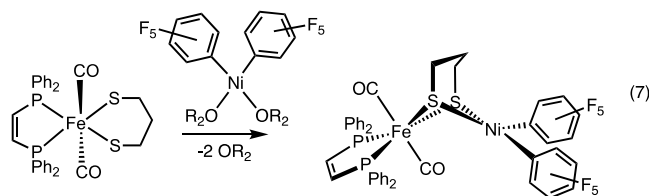


Figure 12. Optimized structures of the low-energy isomers of $\{\text{H}[(\text{dppv})(\text{CO})\text{Fe}(\mu\text{-pdt})]_2\text{Ni}\}^+$. Selected distances (Å): Fe(2)–H, 1.635 in $[\text{H1A}]^+$ and 1.654 in $[\text{H1B}]^+$; Ni(1)–H, 1.745 in $[\text{H1A}]^+$ and 1.643 in $[\text{H1B}]^+$.

complexes with Ni–C sigma bonds. The methodology was revised with a focus on $\text{Ni}(\text{C}_6\text{F}_5)_2(\text{dioxane})_2$, which is known to have labile ether ligands and robust Ni–C bonds.⁵⁰ Indeed, this complex reacted readily with $\text{Fe}(\text{pdt})(\text{CO})_2(\text{dppv})$ to

form a ruby-red 1:1 adduct $(C_6F_5)_2Ni(\mu\text{-pdt})Fe(CO)_2(dppv)$ (eq 7, Figures S69–S71).



The ^{31}P and ^{19}F NMR data are consistent with a C_s -symmetric Ni–Fe complex with a square planar Ni center and octahedral Fe site (Figures S70–S71). X-ray crystallographic characterization confirms these findings (Figure 13).

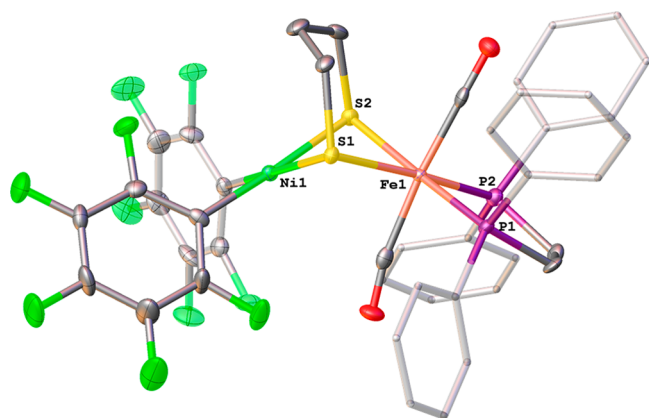


Figure 13. ORTEP diagram (50% probability) of $(C_6F_5)_2Ni(\mu\text{-pdt})Fe(CO)_2(dppv)$. H atoms were removed for clarity. Selected distances (Å): Ni(1)–S(1), 2.2596(8); Ni(1)–S(2), 2.2335(8); Fe(1)–S(1), 2.3313(8); Fe(1)–S(2), 2.3313(7); Fe(1)–P(1), 2.2246(8); Fe(1)–P(2), 2.2183(9).

SUMMARY AND CONCLUSIONS

Many properties of the active site of the [NiFe]-hydrogenases remain to be simulated with models (Figure 1). Addressing these gaps requires the development of new and the evolution of established synthetic methods. This report describes both approaches to complexes with $Ni(\mu\text{-SR})_2Fe$ cores.

The boldest approach to active site models entailed the use of the tetrahedral $[Ni(NS_3)]^-$ building block. The starting complex $[Ni(NS_3)]^-$ is a remarkable example of a robust, air-stable tetrahedral nickel(II) thiolate. Many nickel tri- and tetrathiolates are known, including the iconic $[Ni(SPh)_4]^{2-}$,⁵² but they are either exchange-labile, oligomerize, or both.⁵² The complex $[Ni(NS_3)]^-$ was deployed in an attempt to approximate the geometry of the $Ni(SR)_4$ site, as seen in the enzyme. One barrier to producing $Ni(SR)_2Fe$ ensembles, suggested by the formation of tetrametallic complexes with $[Ni(NS_3)]_2Fe_2$ cores, is the wide S–Ni–S angle in $[Ni(NS_3)]^-$. An associated deficiency in this Ni-containing building block is that the Ni center exhibits no Lewis acidity, which is a requirement for $Ni(II)$ – $Fe(II)$ models.

The active sites of the hydrogenases are chiral owing to the asymmetric distribution of ligands around the nickel centers. Using chiral ancillary ligands, e.g., *R,R*-DIPAMP, represents one method to impose asymmetry. The twisting introduced by the C_2 -symmetric ligand is not however transmitted to the geometry at the Ni site, which adopts a planar NiS_2P_2

coordination sphere. Furthermore, neither the Ni center nor the hydride exhibited any affinity for the methoxy substituent. In the enzyme, water is assumed to bind to $Ni(II)$ and especially $Ni(III)$.⁴ The work does however demonstrate the utility of chiral ligands to probe the stereodynamics of $Ni(SR)_2Fe$ models. In a related modeling effort, phosphine-imine and phosphine-amine ligands were installed in rare examples of models with Ni–N bonds.

The final phase of this study examined nickel-aryl reagents. The original idea was to introduce alkyl/aryl ligands that would be susceptible to protonolysis by thiols. In one case, this approach afforded the first $Ni(SR)_4$ -hydrides. As active site models, these $NiFe_2$ complexes have incorrect metal stoichiometry. Nonetheless DFT calculations support the existence of $Fe-H-Ni(SR)_4$ centers where the geometry at Ni approaches that in the enzyme.¹³ The preparation of $Fe-H-Ni(SR)_4$ centers with terminal thiolates remains an unsolved challenge.

EXPERIMENTAL SECTION

General. Literature procedures were followed for the preparation of $P(SH)_3$ from thiophenol.⁵³ For the preparation of $N(SH)_3$, $N(CH_2C_6H_4-2-Br)_3$ was prepared using an aqueous ammonia method,²⁶ followed by lithiation and sulfidation.^{54,55} $PCH=N^{An}$ was prepared by a modification of the published route,⁵⁶ as described in the Supporting Information. The complexes $Ni(pdt)(dppv)$, $Ni(pdt)(dppv)$, and $Ni(pdt)(dppbz)$ were prepared from the corresponding $NiCl_2$ (diphosphine) by treatment with propanedithiol and 2 equiv of NaOMe in a mixture of CH_2Cl_2 and MeOH. The following organometallic reagents were prepared according to literature procedures: $[CpFe(CO)_2(thf)]BF_4$,⁵⁷ $[Cp^*Fe(CO)(MeCN)_2]BF_4$ and $[Cp^*Fe(CO)(MeCN)_2]BF_4$,⁵⁸ $NiCl_2(DME)$,⁵⁹ $Fe(dppv)(CO)_2Cl_2$,⁶⁰ $Fe_2(CO)_4$,⁶¹ and $Ni(C_6F_5)_2$ (dioxane).⁵⁰ $Fe(pdt)(CO)_2(dppv)$ and $Fe(pdt)(CO)_2(dppbz)$ were prepared as we previously described.⁶² Efforts to improve the yields were fruitless. Other methods have been described recently.⁶³

$Ph_4P[Ni(NS_3)]$. A solution of NaOMe (0.216 g, 4 mmol) in MeOH (10 mL) was added to a slurry of $[NH(SH)_3]^+Cl^-$ (0.420 g, 1 mmol), also in MeOH (20 mL). The resulting homogeneous solution of $N(SNa)_3$ was allowed to stir for 30 min before being evaporated. A solution of this white residue in 10 mL of EtOH was treated with a solution of $NiCl_2 \cdot 6H_2O$ (0.240 g, 1 mmol) in 10 mL of EtOH. The color of the solution immediately changed to dark green. After 1 h, solvent was removed, leaving a green-colored residue of $Na[Ni(NS_3)]$. Alternatively, addition of Ph_4PBr (0.630 g, 1.5 mmol) to the dark green $Na[Ni(NS_3)]$ solution precipitated a green solid. Yield: 662 mg (85%). X-ray quality crystals of $Ph_4P[Ni(NS_3)]$ were obtained from vapor diffusion of pentane into CH_2Cl_2 solution of the complex at $-30^\circ C$. 1H NMR (500 MHz, CD_2Cl_2): δ –11.50, –10.85, 7.70, 7.95, 8.05, 13.33, 19.40, 96.99, 287.43. ^{31}P NMR (202 MHz, CH_2Cl_2): δ 23.58. ESI-MS (negative, CH_2Cl_2): 437.9965 ($[M]^-$, 100%). UV–vis (CH_2Cl_2): $\lambda = 373$ nm ($\epsilon = 6367$ $cm^{-1} M^{-1}$), 435 ($\epsilon = 3681$), 477 ($\epsilon = 3766$), 637 ($\epsilon = 1185$). Anal. Calcd for $C_{46}H_{40}Cl_2NNiP_3$ [$Ph_4P[Ni(NS_3)] \cdot CH_2Cl_2$ (found): C, 63.98 (64.08); H, 4.67 (4.71); N, 1.62 (1.81).

$[Ni(NS_3)Fe(CO)_2Cp]$ and $[Ni(NS_3)Fe(CO)Cp]_2$. A solution of $Na[Ni(NS_3)]$ (0.462 g, 1 mmol) (or $Ph_4P[Ni(NS_3)]$ (0.779 g, 1 mmol)) in 15 mL of THF was treated with a solution of $[CpFe(CO)_2(thf)]BF_4$ (0.336 g, 1 mmol) in 15 mL of THF. The resulting dark brownish solution was stirred for 2 h. Addition of pentane to the reaction mixture precipitated $[Ni(NS_3)Fe(CO)_2Cp]$ as a brown solid (IR (THF): $\nu_{CO} = 2046, 2002$ cm^{-1}). A THF solution of this crude product was stirred for a few days in daylight. Vapor diffusion of pentane into the THF solution of the complex yielded crude $[Ni(NS_3)Fe(CO)Cp]_2$. This complex was purified by extraction into CH_2Cl_2 . The filtered extract was evaporated to dryness to yield the desired product. This $[Ni(NS_3)Fe(CO)Cp]_2$ complex can

also be synthesized upon reaction between $\text{Na}[\text{Ni}(\text{NS}_3)]$ (0.462 g, 1 mmol) (or $\text{Ph}_4\text{P}[\text{Ni}(\text{NS}_3)]$ (0.779 g, 1 mmol)) and $[\text{CpFe}(\text{CO})(\text{MeCN})_2]\text{BF}_4$ (0.318 g, 1 mmol) in 20 mL of CH_2Cl_2 . After 1 day, the solution was filtered, and the filtrate was evaporated, leaving a residue of $[\text{Ni}(\text{NS}_3)\text{Fe}(\text{CO})\text{Cp}]_2$. Low quality crystals could be obtained by layering a CH_2Cl_2 solution of the complex with pentane in an NMR tube at room temperature. Yield: 441 mg (75%). IR (CH_2Cl_2): $\nu_{\text{CO}} = 1957 \text{ cm}^{-1}$. ESI-MS (positive, CH_2Cl_2): 1173.9290 ($[\text{M}]^+$, 100%). Anal. Calcd for $\text{C}_{57}\text{H}_{52}\text{Cl}_6\text{Fe}_2\text{N}_2\text{Ni}_2\text{O}_2\text{S}_6$ $[[\text{Ni}(\text{NS}_3)\text{Fe}(\text{CO})\text{Cp}]_2 \cdot 3\text{CH}_2\text{Cl}_2]$ (found): C, 47.84 (47.52); H, 3.66 (3.46); N, 1.96 (1.67).

$\text{Ni}(\text{NS}_3)\text{Fe}(\text{CO})\text{Cp}^*$. A solution of $\text{Na}[\text{Ni}(\text{NS}_3)]$ (0.462 g, 1 mmol) (or $\text{Ph}_4\text{P}[\text{Ni}(\text{NS}_3)]$ (0.779 g, 1 mmol)) in 15 mL of CH_2Cl_2 was treated with a solution of $[\text{Cp}^*\text{Fe}(\text{CO})(\text{MeCN})_2]\text{BF}_4$ (0.388 g, 1 mmol) in 15 mL of CH_2Cl_2 . After being stirred for 24 h, the reaction solution was filtered, and the filtrate was evaporated to leave a brown residue. Yield: 461 mg (70%). IR (CH_2Cl_2): $\nu_{\text{CO}} = 1954, 1925 \text{ cm}^{-1}$. ESI-MS (CH_2Cl_2): 657.0421 ($[\text{M}]^+$, 100%), 629.0474 ($[\text{M}-\text{CO}]^+$, 77%). Anal. Calcd for $\text{C}_{36}\text{H}_{41}\text{Cl}_3\text{FeNiNiO}_3$ $[[\text{Ni}(\text{NS}_3)\text{Fe}(\text{CO})\text{Cp}^*] \cdot 4\text{CH}_2\text{Cl}_2]$ (found): C, 43.32 (43.28); H, 4.14 (4.34); N, 1.40 (1.92).

Reaction of $[\text{CpFe}(\text{CO})_2(\text{thf})]\text{BF}_4$ with $\text{Ni}(\text{pdt})(\text{dppe})$. A solution of $[\text{CpFe}(\text{CO})_2(\text{thf})]\text{BF}_4$ (0.336 g, 1 mmol) in 15 mL of CH_2Cl_2 was added to a solution of $\text{Ni}(\text{pdt})(\text{dppe})$ (0.563 g, 1 mmol) in 25 mL of CH_2Cl_2 . The reaction mixture was stirred for 72 h and then filtered. Dilution of the filtrate with pentane precipitated a mixture of $[\text{Cp}(\text{CO})\text{Fe}(\mu\text{-pdt})\text{Ni}(\text{dppe})]\text{BF}_4$ and $[\text{Ni}_2(\mu\text{-pdt})(\mu\text{-Cl})(\text{dppe})_2]\text{BF}_4$, which were identified spectroscopically. ^{31}P NMR (202 MHz, CH_2Cl_2): δ 56.58, 56.95, 57.81; IR (CH_2Cl_2): $\nu_{\text{CO}} = 1953 \text{ cm}^{-1}$. X-ray quality crystals of $[\text{Cp}(\text{CO})\text{Fe}(\mu\text{-pdt})\text{Ni}(\text{dppe})]\text{BF}_4$ were obtained by vapor diffusion of pentane into CH_2Cl_2 solution of the mixture. When the reaction was repeated using THF in place of CH_2Cl_2 , the pentane-precipitate was a mixture of $[\text{Cp}(\text{CO})\text{Fe}(\mu\text{-pdt})\text{Ni}(\text{dppe})]\text{BF}_4$ and $[\text{CpFe}(\text{CO})(\text{dppe})]\text{BF}_4$, which were identified spectroscopically. ^1H NMR (500 MHz, CH_2Cl_2): δ 2.51–2.67 (2H, m), 2.67–2.82 (2H, m), 4.75 (5H, s), 7.11–7.22 (4H, m), 7.45 (4H, d, $J = 6.71$), 7.48–7.64 (12H, m). ^{31}P NMR (202 MHz, THF): δ 92.93. IR (CH_2Cl_2): $\nu_{\text{CO}} = 1980 \text{ cm}^{-1}$.

Reaction of $[\text{CpFe}(\text{CO})_2(\text{thf})]\text{BF}_4$ with $\text{Ni}(\text{pdt})(\text{dppv})$. A solution of $[\text{CpFe}(\text{CO})_2(\text{thf})]\text{BF}_4$ (0.336 g, 1 mmol) in 15 mL of CH_2Cl_2 was added into a solution of $\text{Ni}(\text{dppv})(\text{pdt})$ (0.561 g, 1 mmol) in 25 mL of CH_2Cl_2 . After stirring for 3 days, the mixture was filtered, and the filtrate was diluted with pentane to precipitate a mixture of $[\text{Cp}(\text{CO})\text{Fe}(\mu\text{-pdt})\text{Ni}(\text{dppv})]\text{BF}_4$ and $[\text{Ni}_2(\text{pdt})(\mu\text{-Cl})(\text{dppv})_2]\text{BF}_4$, which were identified spectroscopically. ^{31}P NMR (202 MHz, CH_2Cl_2): δ 64.61, 65.97, 66.58, 59.07. The last two signals are assigned to $[\text{Cp}(\text{CO})\text{Fe}(\mu\text{-pdt})\text{Ni}(\text{dppv})]\text{BF}_4$ and $[\text{Ni}_2(\text{pdt})(\mu\text{-Cl})(\text{dppv})_2]\text{BF}_4$, respectively. When the same reaction was repeated in THF, the exclusive product precipitated with pentane was $[\text{Cp}(\text{CO})\text{Fe}(\mu\text{-pdt})\text{Ni}(\text{dppv})]\text{BF}_4$. Yield: 558 mg (70%). ^{31}P NMR (202 MHz, THF): δ 64.6 (major), 66.0, 66.6. (weak) IR (THF): $\nu_{\text{CO}} = 1946 \text{ cm}^{-1}$.

$[\text{Cp}(\text{CO})\text{Fe}(\mu\text{-pdt})\text{Ni}(\text{dppbz})]\text{BF}_4$. A solution of $[\text{CpFe}(\text{CO})(\text{MeCN})_2]\text{BF}_4$ (0.032 g, 0.1 mmol) in 5 mL of THF was added into a solution of $\text{Ni}(\text{pdt})(\text{dppbz})$ (0.061 g, 0.1 mmol) in 5 mL of THF. As the reaction mixture stirred for 24 h, green solid precipitated. X-ray quality crystals were grown by vapor diffusion of pentane into CH_2Cl_2 solution of the salt at -29°C . Yield: 72 mg (85%). ^{31}P NMR (202 MHz, CH_2Cl_2): δ 56.4 (major), 57.3 (small peak, may be due to a stereoisomer based on the position of Cp and CO) IR (CH_2Cl_2): $\nu_{\text{CO}} = 1953 \text{ cm}^{-1}$. ESI-MS (positive, CH_2Cl_2): 759.0300 ($[\text{M}]^+$), 731.0234 ($[\text{M}-\text{CO}]^+$). Anal. Calcd for $\text{C}_{39.5}\text{H}_{36}\text{BCl}_4\text{FeNiO}_2\text{P}_2$ $[[\text{Cp}(\text{CO})\text{Fe}(\mu\text{-pdt})\text{Ni}(\text{dppbz})]\text{BF}_4] \cdot 0.5\text{CH}_2\text{Cl}_2]$ (found): C, 53.33 (53.8); H, 4.08 (4.52).

$\text{NiCl}_2(\text{R,R-DIPAMP})$. A slurry of NiCl_2 (0.65 mmol, 85 mg) and R,R-DIPAMP (0.65 mmol, 300 mg) in 5 mL of EtOH was heated at reflux for 15 min. After cooling the mixture to 0°C , an orange solid precipitate was collected and washed with EtOH and Et_2O . Yield: 360 mg (94%). Anal. Calcd for $\text{C}_{28.2}\text{H}_{28.4}\text{Cl}_2\text{Ni}_2\text{O}_2\text{P}_2$ $[\text{NiCl}_2(\text{R,R-DIPAMP}) \cdot 0.2\text{CH}_2\text{Cl}_2]$ (found): C, 55.98 (55.97); H, 4.73 (4.6).

$\text{Ni}(\text{pdt})(\text{R,R-DIPAMP})$. A suspension of $\text{NiCl}_2(\text{R,R-DIPAMP})$ (0.61 mmol, 360 mg) and 1,3-propanedithiol (0.61 mmol) in CH_2Cl_2 was treated dropwise with a solution of NaOMe (1.22 mmol) in 1 mL of MeOH. The resulting mixture was stirred for 30 min. Solvent was removed, and the residue was extracted into CH_2Cl_2 . The extract was filtered through a pad of Celite and then evaporated to afford $\text{Ni}(\text{pdt})(\text{R,R-DIPAMP})$ as a brown-red solid. Yield: 350 mg (92%). ^1H NMR (500 MHz, CD_2Cl_2): δ 8.33 (s, 4H), 7.58 (s, 6H), 7.38 (t, $J = 7.7$ Hz, 2H), 6.99–6.79 (m, 6H), 3.39 (s, 6H), 2.41–2.35 (m, 4H), 2.30–2.25 (m, 2H), 2.24–2.20 (m, 2H), 1.89 (q, $J = 6.0$ Hz, 2H). ^{31}P NMR (202 MHz, CD_2Cl_2): δ 53.4 (s).

$[(\text{R,R-DIPAMP})\text{Ni}(\mu\text{-pdt})(\text{H})\text{Fe}(\text{CO})_3]\text{BARF}_4$. At -80°C , a stirred mixture of $\text{Fe}_2(\text{CO})_4$ (236 mg, 0.56 mmol) and $\text{Ni}(\text{pdt})(\text{R,R-DIPAMP})$ (350 mg, 0.56 mmol) was treated with 7 mL of CH_2Cl_2 , resulting in a dark brown homogeneous solution. After 2 min, the IR spectrum of the mixture showed $\nu_{\text{CO}} = 2094, 2076, 2050, \text{ and } 2021 \text{ cm}^{-1}$, consistent with the formation of the μ -iodo intermediate $[(\text{R,R-DIPAMP})\text{Ni}(\mu\text{-pdt})(\text{I})\text{Fe}(\text{CO})_3]^+$. The cold reaction mixture was treated with 2 equiv (212 mg, 1.12 mmol) of Cp_2Co . The reaction solution became dark green. After stirring for 1 h at room temperature, the reaction mixture was evaporated, and the resulting green solid was washed with MeCN. The solid was extracted into 5 mL of CH_2Cl_2 , and the extract was filtered through Celite. The CH_2Cl_2 solution was evaporated, leaving $(\text{R,R-DIPAMP})\text{Ni}(\mu\text{-pdt})\text{Fe}(\text{CO})_3$ as a green solid. Yield: 215 mg (50%). ^1H NMR (500 MHz, CD_2Cl_2): δ 7.78 (s, 6H), 7.37 (s, 8H), 7.13–6.73 (m, 4H), 3.67 (s, 6H), 2.62 (s, 2H), 2.43–2.27 (m, 4H), 2.05–1.61 (m, 4H). ^{31}P NMR (202 MHz, CD_2Cl_2): δ 60.0 (s). IR (CH_2Cl_2): $\nu_{\text{CO}} = 2024, 1950 \text{ cm}^{-1}$. A stirred solution of $(\text{R,R-DIPAMP})\text{Ni}(\mu\text{-pdt})\text{Fe}(\text{CO})_3$ (100 mg, 0.13 mmol) in 3 mL of CH_2Cl_2 was treated with $\text{H}(\text{OEt}_2)\text{BARF}_4$ (121 mg, 0.12 mmol). An immediate color change from green to red was observed. The solution was concentrated to ~ 1 mL. The concentrate was layered with pentane and cooled to -20°C to give $[(\text{R,R-DIPAMP})\text{Ni}(\mu\text{-pdt})(\text{H})\text{Fe}(\text{CO})_3]\text{BARF}_4$ as red colored solid. Yield: 82 mg (42%). ^{31}P NMR (202 MHz, CD_2Cl_2): δ 66.8 (br. s). ^1H NMR (500 MHz, CD_2Cl_2): δ -3.06 (s, 1H, hydride). IR (CH_2Cl_2): $\nu_{\text{CO}} = 2078, 2016 \text{ cm}^{-1}$. Anal. Calcd for $\text{C}_{67}\text{H}_{49}\text{Cl}_2\text{BF}_4\text{FeNiO}_3\text{P}_2\text{S}_2$ $[(\text{R,R-DIPAMP})\text{Ni}(\mu\text{-pdt})(\text{H})\text{Fe}(\text{CO})_3]\text{BARF}_4 \cdot \text{CH}_2\text{Cl}_2]$ (found): C, 46.99 (47.31); H, 2.88 (2.89).

$[\text{NiCl}_2(\text{PCH}=\text{N}^{\text{An}})]_2$. A slurry of $\text{NiCl}_2(\text{DME})$ (0.220 g, 1 mmol) in 15 mL of CH_2Cl_2 was added into a stirred solution of $\text{PCH}=\text{N}^{\text{An}}$ (0.395 g, 1 mmol) in 20 mL of CH_2Cl_2 . After 2 h, the solution was concentrated to 10 mL. Dilution with pentane gave yellow-brown crystals. X-ray quality crystals were obtained upon layering a CH_2Cl_2 solution of the complex with pentane. Yield: 420 mg (80%). Anal. Calcd for $\text{C}_{53}\text{H}_{46}\text{Cl}_6\text{N}_2\text{Ni}_2\text{O}_2\text{P}_2$ $[[\text{NiCl}_2(\text{PCH}=\text{N}^{\text{An}})]_2 \cdot \text{CH}_2\text{Cl}_2]$ (found): C, 56.09 (55.87); H, 4.09 (3.81); N, 2.47 (2.49).

$\text{PCH}_2\text{NH}^{\text{An}}$. To a solution of $\text{PCH}=\text{N}^{\text{An}}$ (0.490 g, 1.24 mmol) in 30 mL of MeOH at 0°C was added NaBH_4 (0.180 g, 4.76 mmol) over the course of a few minutes. After the addition was complete, the reaction mixture was stirred for 15 min. The reaction mixture was treated with aqueous 1 M NaOH solution (5 mL). The mixture was extracted into CH_2Cl_2 . After drying the extract over MgSO_4 , solvent was removed leaving a colorless oil. Yield: 443 mg (90%). ^{31}P NMR (202 MHz, CD_2Cl_2): δ -15.88 (s). ^1H NMR (500 MHz, CD_2Cl_2): 3.74 (s, 3H), 4.48 (d, 2H), 6.41 (d, 2H), 6.72 (d, 2H), 6.95 (t, 1H), 7.21 (t, 1H), 7.29–7.38 (m, 12 H), 7.53 (q, 1H).

$[\text{NiCl}_2(\text{PCH}_2\text{NH}^{\text{An}})]_2$. A slurry of $\text{NiCl}_2(\text{DME})$ (0.110 g, 0.5 mmol) in 15 mL of CH_2Cl_2 was added into a solution of $\text{PCH}_2\text{NH}^{\text{An}}$ (0.199 g, 0.5 mmol) in 20 mL of CH_2Cl_2 . From the initially homogeneous solution precipitated a yellow solid. The reaction was continued for 2 h before the solid was collected by filtration. This compound is insoluble in CH_2Cl_2 but soluble in THF. X-ray quality crystals were obtained upon vapor diffusion of pentane into THF solution of the complex at room temp. Yield: 210 mg (80%). Anal. Calcd for $\text{C}_{53}\text{H}_{50}\text{Cl}_6\text{N}_2\text{Ni}_2\text{O}_2\text{P}_2$ $[[\text{NiCl}_2(\text{PCH}_2\text{NH}^{\text{An}})]_2 \cdot \text{CH}_2\text{Cl}_2]$ (found): C, 55.89 (56.33); H, 4.42 (5.00); N, 2.46 (2.44).

$[(\text{PCH}=\text{N}^{\text{An}})\text{Ni}(\mu\text{-pdt})\text{CFe}(\text{dppbz})(\text{CO})]\text{BF}_4$. A slurry of $[\text{NiCl}_2(\text{PCH}=\text{N}^{\text{An}})]_2$ (0.050 g, 0.05 mmol) in 10 mL of acetone was treated with a solution of NaBF_4 (0.017 g, 0.15 mmol) in 10 mL

of acetone followed by a slurry of $\text{Fe}(\text{pdt})(\text{CO})_2(\text{dppbz})$ (0.066 g, 0.1 mmol) also in 10 mL of acetone. The mixture immediately became dark brown. After stirring the mixture for 2 h at 0 °C, solvent was removed under a vacuum. The solid residue was extracted into CH_2Cl_2 , and this extract was filtered through glass wool. The filtrate was evaporated to give a brown-colored solid. Crystals were obtained from vapor diffusion of pentane into a CH_2Cl_2 solution of the salt at -30 °C. Yield: 115 mg (95%). IR (CH_2Cl_2): $\nu_{\text{CO}} = 1946 \text{ cm}^{-1}$. ESI-MS (positive, CH_2Cl_2): 1124.1044 $[\text{M}]^+$, 1096.1278 $[\text{M}-\text{CO}]^+$. ^{31}P NMR (202 MHz, CH_2Cl_2): δ 72.66 (dd, 1P, Fe-P), 67.80 (dd, 1P, Fe-P), 19.43 (dd, 1P, Ni-P). ^1H NMR (500 MHz, CD_2Cl_2): δ 7.76–6.54 (overlapping signals, 43H), 3.80 (s, 3H), 3.62 (dt, $J = 13.73, 4.58$ Hz, 1 H), 2.89 (d, $J = 13.73$ Hz, 1 H), 2.27 (d, $J = 13.73$ Hz, 1 H), 2.01–2.10 (m, 1 H), 1.92–2.01 (m, 1 H), 1.86 (d, $J = 7.63$ Hz, 1 H). Anal. Calcd for $\text{C}_{62.5}\text{H}_{57}\text{BCl}_5\text{F}_4\text{FeNNiO}_2\text{P}_3\text{S}_2$ [(PCH=N^{An})Ni(μ -pdt)ClFe(dppbz)(CO)]BF₄·2.5CH₂Cl₂ (found): C, 52.67 (52.39); H, 4.03 (4.2); N, 0.98 (1.0).

[(PCH=N^{An})Ni(μ -pdt)(H)Fe(dppbz)(CO)]BF₄. A solution of Cp*₂Co (0.066 g, 0.2 mmol) in 5 mL of THF was added into a slurry of [(PCH=N^{An})Ni(μ -pdt)ClFe(dppbz)(CO)]BF₄ (0.121 g, 0.1 mmol) in 5 mL of THF. The resulting mixture was stirred for 2 h at room temperature. The yellow solid precipitate [(Cp*₂Co)Cl/[Cp*₂Co]BF₄] was filtered off. The filtrate was evaporated to dryness to obtain the (PCH=N^{An})Ni(μ -pdt)Fe(dppbz)(CO) as a brown solid. This compound is soluble in THF, toluene, and CH_2Cl_2 . IR (CH_2Cl_2): $\nu_{\text{CO}} = 1919 \text{ cm}^{-1}$. ^{31}P NMR (202 MHz, THF): δ 88.35 (dd, 1P, Fe-P), 80.74 (dd, 1P, Fe-P), 36.13 (q, 1P, Ni-P). ^1H NMR (500 MHz, THF-*d*₆): δ 8.22–6.16 (overlapping signals, 43H), 3.49 (s, 3H), 2.17 (m, 1H), 1.92 (m, 1H), 1.84 (m, 1H), 1.66 (m, 1H), 1.13 (m, 1H), 1.04 (m, 1H). Crude (PCH=N^{An})Ni(μ -pdt)Fe(dppbz)(CO) (0.087 g, 0.08 mmol) was dissolved in 10 mL of THF, and HBF₄·Et₂O (11 μL , 0.08 mmol) was added dropwise to this solution. The resulting dark brown mixture was stirred for 2 h. The solvent was evaporated to dryness to obtain [(PCH=N^{An})Ni(μ -pdt)(H)Fe(dppbz)(CO)]BF₄. Crystals were obtained upon vapor diffusion of pentane into CH_2Cl_2 solution of the salt. Yield: 85 mg (90%). IR (CH_2Cl_2): $\nu_{\text{CO}} = 1945 \text{ cm}^{-1}$. ESI-MS (positive, CH_2Cl_2): 1090.1417 $[\text{M}]^+$, 1062.1503 $[\text{M}-\text{CO}]^+$. ^{31}P NMR (202 MHz, THF): δ 94.47 (1P, Fe-P), 91.58 (1P, Fe-P), 76.78–77.30 (2P, Fe-P), 28.01 (d, 1P, Ni-P), 21.50 (t, 1P, Ni-P). ^{31}P NMR (202 MHz, CD_2Cl_2): δ 94.55 (1P, Fe-P), 91.01 (1P, Fe-P), 75.83 (0.5P, Fe-P), 72.92 (0.5P, Fe-P), 26.75 (1P, Ni-P), 19.83 (0.5P, Ni-P). ^1H NMR (CD_2Cl_2): δ -0.66 (t, hydride, 1H). Anal. Calcd for $\text{C}_{61}\text{H}_{55}\text{BCl}_5\text{F}_4\text{FeNNiO}_2\text{P}_3\text{S}_2$ [(PCH=N^{An})Ni(μ -pdt)(H)Fe(dppbz)(CO)]BF₄·CH₂Cl₂ (found): C, 57.99 (58.13); H, 4.39 (5.05); N, 1.11 (1.12).

[(PCH₂NH^{An})Ni(μ -pdt)ClFe(dppbz)(CO)]BF₄. A slurry of Fe(pdt)(CO)₂(dppbz) (0.066 g, 0.1 mmol) in 10 mL of acetone was treated with a slurry of [NiCl₂(PCH₂NH^{An})₂] (0.050 g, 0.05 mmol) in 10 mL of acetone and a solution of NaBF₄ (0.017 g, 0.15 mmol) also in 10 mL of acetone. The solution immediately turned dark brown. The resulting mixture was stirred for 2 h at 0 °C. Solvent was removed, and the solid residue was extracted with CH_2Cl_2 . After filtering through glass wool, this extract was evaporated, leaving brown-black solid product. Yield: 110 mg (91%). IR (CH_2Cl_2): $\nu_{\text{CO}} = 1949 \text{ cm}^{-1}$. ESI-MS (positive, CH_2Cl_2): 1126.1201 $[\text{M}]^+$, 1098.1071 $[\text{M}-\text{CO}]^+$. ^{31}P NMR (202 MHz, CH_2Cl_2): δ 74.07 (dd, 1P, Fe-P), 71.43 (dd, 1P, Fe-P), -3.25 (dd, 1P, Ni-P). ^1H NMR (500 MHz, CD_2Cl_2): δ 7.82–6.50 (overlapping signals, 42H), 3.89–4.05 (m, 2 H), 3.78 (s, 3H), 3.50 (m, 1 H), 3.04 (m, 1 H), 2.49 (d, $J = 9.16$ Hz, 1 H), 2.04 (m, 1 H), 1.90 (m, 1 H), 1.44 (m, 1 H), 0.62 (d, $J = 7.63$ Hz, 1 H). Anal. Calcd for $\text{C}_{61}\text{H}_{56}\text{BCl}_5\text{F}_4\text{FeNNiO}_2\text{P}_3\text{S}_2$ [(PCH₂NH^{An})Ni(μ -pdt)ClFe(dppbz)(CO)]BF₄·CH₂Cl₂ (found): C, 56.37 (56.32); H, 4.34 (4.56); N, 1.08 (1.18).

[(dppv)(CO)Fe(μ -pdt)]₂Ni. To a solution of Fe(pdt)(CO)₂(dppv) (1.02 g, 1.66 mmol, 1 equiv) in 10 mL of THF was added a solution of Ni(*o*-tol)Cl(tmeda) (0.50 g, 1.66 mmol, 1 equiv) in 5 mL of THF. The reaction was stirred at room temperature for 8 h. A dark brown solution developed. The solvent was removed under a vacuum. The solid residue was extracted into 3 mL of CH_2Cl_2 , and this extract was filtered through a 5 × 15 cm column of silica gel using

additional CH_2Cl_2 as an eluent. The brown-colored band was collected and reduced in volume. Addition of 60 mL of pentane to the concentrated CH_2Cl_2 solution precipitated [(dppv)(CO)Fe(μ -pdt)]₂Ni as a brown solid. Yield: 0.362 g (35%). Vapor diffusion of pentane into a concentrated solution of [(dppv)(CO)Fe(μ -pdt)]₂Ni in CH_2Cl_2 gave red-orange prisms suitable for X-ray crystallography. ^1H NMR (500 MHz, C₆D₆): δ 8.34 (br s, 8H), 7.74–7.55 (m, 12H), 7.32 (br s, 8H), 7.11 (m, 4H), 7.03 (m, 8H), 6.97 (m, 4H), 2.16–1.77 (m, 8H), 1.32–1.07 (m, 4H). $^{31}\text{P}\{^1\text{H}\}$ NMR (202 MHz, C₆D₆): δ 100.19 (br s, 2P), 81.51 (br s, 2P). IR (THF): $\nu_{\text{CO}} = 1914 \text{ cm}^{-1}$. Anal. Calcd for C₆₀H₅₈Fe₂NiO₂P₄S₄: C, 58.42; H, 4.74. Found: C, 57.65; H, 4.44.

{[H(dppv)(CO)Fe(μ -pdt)]₂Ni}BF₄. A solution of [(dppv)(CO)Fe(μ -pdt)]₂Ni (200 mg, 1.62×10^{-4} mmol, 1 equiv) in 4 mL of CH_2Cl_2 was treated with HBF₄·Et₂O (22 μL , 26 mg, 1.62×10^{-4} mol, 1 equiv). The mixture was stirred at room temperature for 30 min. A dark red solution developed. The solvent was removed under a vacuum. The solid residue was washed with dry Et₂O (3 × 5 mL) and dried under a vacuum. Crystals of this were grown by vapor diffusion of pentane into CH_2Cl_2 solutions of the salt at room temperature. Yield: 152 mg (71%). ^1H NMR (500 MHz, CD_2Cl_2 , basal–basal isomer, -60 °C): δ 8.27 (ddd, $J = 85, 45, 12$ Hz, 4H), 7.73 (s, 4H), 7.32 (br s, 8H), 7.64–7.05 (m, 36H), 2.52–1.22 (overlapping signals, 6H), 1.10 (s, 2H), 0.31 (br s, 1H), 0.25 (br s, 2H), -0.28 (br s, 1H), -5.10 (br s, 1H). ^1H NMR (500 MHz, CD_2Cl_2 , mixture of isomers, 20 °C): δ 8.56–7.05 (overlapping signals, 40H), 2.48 (m, 0.74 H), 2.04 (t, $J = 13$ Hz, 0.91H), 1.97 (m, 0.44H), 1.75 (m, 2.75H), 1.59 (m, 1.31H), 1.27 (m, 0.8H), 1.15 (m, 0.75H), 1.08 (m, 1.36H), 0.82 (m, 1.63H), 0.51 (m, 0.49H), 0.27 (m, 0.77H), -0.15 (q, $J = 13$ Hz), -4.87 (t, $J = 38$ Hz, 0.15H), -6.67 (br s, 0.23H), -15.50 (s, 0.36H). $^{31}\text{P}\{^1\text{H}\}$ NMR (202 MHz, CD_2Cl_2 , 20 °C): δ 95.23 (br s, 2P, apical–basal isomer), 91.49 (br s, 2P, apical–basal isomer), 87.43 (s, 4P, Ni–H), 86.72 (s, 2P, basal–basal isomer), 71.70 (s, 2P, basal–basal isomer). IR (THF): $\nu_{\text{CO}} = 1965, 1943 \text{ cm}^{-1}$. Anal. Calcd for C₆₁H₅₅B C₄F₄Fe₂NiO₂P₄S₄: C, 52.17; H, 4.23. Found: C 52.09; H, 4.35. [H(dppv)(CO)Fe(μ -pdt)]₂Ni}BAR^F₄ was prepared similarly. ^1H NMR (500 MHz, CD_2Cl_2 , mixture of isomers, 20 °C): δ 8.56–7.05 (overlapping signals, 48H), 2.48 (m, 0.74 H), 2.04 (t, $J = 13$ Hz, 0.91H), 1.97 (m, 0.44H), 1.75 (m, 2.75H), 1.59 (m, 1.31H), 1.27 (m, 0.8H), 1.15 (m, 0.75H), 1.08 (m, 1.36H), 0.82 (m, 1.63H), 0.51 (m, 0.49H), 0.27 (m, 0.77H), -0.15 (q, $J = 13$ Hz), -4.87 (t, $J = 38$ Hz, 0.15H), -6.67 (br s, 0.23H), -15.50 (s, 0.36H). $^{31}\text{P}\{^1\text{H}\}$ NMR (202 MHz, CD_2Cl_2 , 20 °C): δ 95.23 (br s, 2P, apical–basal isomer), 91.49 (br s, 2P, apical–basal isomer), 87.43 (s, 4P, Ni–H), 86.72 (s, 2P, basal–basal isomer), 71.70 (s, 2P, basal–basal isomer). IR (THF): $\nu_{\text{CO}} = 1965, 1943 \text{ cm}^{-1}$.

(C₆F₅)₂Ni(μ -pdt)Fe(CO)₂(dppv). In the glovebox a solution of Fe(pdt)(CO)₂(dppv) (370.0 mg, 0.602 mmol) in 30 mL of THF was added dropwise to a stirred solution of Ni(C₆F₅)₂(dioxane)₂ (342.5 mg, 0.602 mmol) in 10 mL of THF over 20 min at room temperature. The solution quickly changed from orange to a very dark red. The reaction was judged complete based on ^{31}P NMR measurements. The volume of the reaction mixture was reduced to ~10 mL under vacuum. Addition of 20 mL of pentane to this filtrate produced a bright red powder. Slow diffusion of pentane into a THF solution of the complex resulted in long ruby-red needles. Yield: 480 mg (79%). ^1H NMR (500 MHz, THF-*d*₈, 20 °C): δ 8.56–7.05 (overlapping signals, 48H), 2.48 (m, 0.74 H), 2.04 (t, $J = 13$ Hz, 0.91H), 1.97 (m, 0.44H), 1.75 (m, 2.75H), 1.59 (m, 1.31H), 1.27 (m, 0.8H), 1.15 (m, 0.75H), 1.08 (m, 1.36H), 0.82 (m, 1.63H), 0.51 (m, 0.49H), 0.27 (m, 0.77H), -0.15 (q, $J = 13$ Hz), -4.87 (t, $J = 38$ Hz, 0.15H), -6.67 (br s, 0.23H), -15.50 (s, 0.36H). $^{19}\text{F}\{^1\text{H}\}$ NMR (470.4 MHz, THF-*d*₈, 20 °C): δ 119.2 (d, $J = 30.8$ Hz, 2F), 120.8 (d, $J = 30.8$ Hz, 2F), 169.75 (t, $J = 20.2$ Hz, 2F), 171.0 (br, 2F), 171.2 (br, 2F). $^{31}\text{P}\{^1\text{H}\}$ NMR (202 MHz, *d*₈-THF, 20 °C): δ 70.5 (s, 2P). IR (THF): $\nu_{\text{CO}} = 2059, 1990 \text{ cm}^{-1}$. Anal. Calcd for C₄₃H₂₈F₁₀FeNiO₂P₂S₂: C, 51.27; H, 2.80. Found: C 50.95; H, 3.00.

X-ray Crystallographic Determinations. Crystallographic Data for Ph₄P[Ni(NS₃)], [Cp(CO)Fe(μ -pdt)Ni(dppbz)]BF₄, [(R,R-DIPAMP)Ni(μ -pdt)(H)Fe(CO)₃]BAR^F₄, [NiCl₂(PCH=N^{An})₂,

$[\text{NiCl}_2(\text{PCH}_2\text{NH}^{\text{An}})]_2$, $[(\text{dppv})(\text{CO})\text{Fe}(\mu\text{-pdt})_2]\text{Ni}$, $\{\text{H}[(\text{dppv})(\text{CO})\text{Fe}(\mu\text{-pdt})_2]\text{Ni}\}\text{BF}_4$, and $(\text{C}_6\text{F}_5)_2\text{Ni}(\mu\text{-pdt})\text{Fe}(\text{CO})_2(\text{dppv})$ were collected on a Bruker D8 Venture instrument equipped with a four-circle kappa diffractometer and Photon 100 detector. An $I\mu\text{s}$ microfocus Mo ($\lambda = 0.71073 \text{ \AA}$) source supplied the multimirror monochromated incident beam. The samples were mounted on a 0.3 mm loop with the minimal amount of Paratone-N oil. Data were collected as a series of φ and/or ω scans. Data were collected at 100 K and integrated and filtered for statistical outliers using SAINT,⁶⁴ and corrected for absorption by multiscan methods using SADABS⁶⁵ v2014/7. The structures were phased using direct methods or intrinsic phasing methods and then refined with the SHELX software package SHELX-2014-7.⁶⁶

Density Functional Theory (DFT). Computations were carried out according to the TZVP/B97-D scheme, as implemented in the TURBOMOLE 7.2 programs suite.^{67–69} The pure B97-D functional, which intrinsically accounts for dispersive effects, was chosen since it proved to reliably reproduce both geometries and reactive behavior of hydrogenase-like models.⁷⁰ The resolution-of-the-identity (RI) technique was used to reduce the computational costs deriving by the treatment of the classical electron–electron repulsive contribution to the total energy.⁷¹ Both low ($S = 0$) and high ($S = 1$) spin forms of $[(\text{dppv})(\text{CO})\text{Fe}(\mu\text{-pdt})_2]\text{Ni}$ have been characterized. With the attempt of localizing opposite spins of the monodeterminant wave function in different parts of the molecule, the Broken Symmetry approximation has been adopted, to detect (eventual) antiferromagnetic spin couplings.⁷² Nuclear magnetic shielding tensors for ^1H NMR chemical shifts were computed according to the Gauge Including Atomic Orbital (GIAO) method^{73,74} on TZVP/BP86 geometries, a very popular scheme for the reproduction of spectroscopic and stereoelectronic features of transition metal complexes relevant to hydrogenases.^{63,75,76}

■ ASSOCIATED CONTENT

● Supporting Information

The Supporting Information is available free of charge on the ACS Publications website at DOI: 10.1021/acs.inorgchem.8b02991.

Listings of NMR and IR spectra, cyclic voltammograms, mass spectra, DFT coordinates, selected reaction schemes and experiments (PDF)

Accession Codes

CCDC 1527147–1527148 and 1873034–1873039 contain the supplementary crystallographic data for this paper. These data can be obtained free of charge via www.ccdc.cam.ac.uk/data_request/cif, or by emailing data_request@ccdc.cam.ac.uk, or by contacting The Cambridge Crystallographic Data Centre, 12 Union Road, Cambridge CB2 1EZ, UK; fax: +44 1223 336033.

■ AUTHOR INFORMATION

Corresponding Author

*E-mail: rauchfuz@illinois.edu.

ORCID

Noémie Lalaoui: 0000-0002-1313-2876

Toby J. Woods: 0000-0002-1737-811X

Thomas B. Rauchfuss: 0000-0003-2547-5128

Notes

The authors declare no competing financial interest.

■ ACKNOWLEDGMENTS

This work was supported by GM-61153 from the National Institutes of Health. We thank Professor S. A. Koch for helpful comments on his group's results on $[\text{Ni}(\text{NS}_3)]^-$.

■ REFERENCES

- (1) Lubitz, W.; Ogata, H.; Rüdiger, O.; Reijerse, E. Hydrogenases. *Chem. Rev.* **2014**, *114*, 4081–4148.
- (2) Ogo, S. H_2 and O_2 Activation by [NiFe]hydrogenases - Insights from Model Complexes. *Coord. Chem. Rev.* **2017**, *334*, 43–53.
- (3) Schilter, D.; Camara, J. M.; Huynh, M. T.; Hammes-Schiffer, S.; Rauchfuss, T. B. Hydrogenase Enzymes and Their Synthetic Models: The Role of Metal Hydrides. *Chem. Rev.* **2016**, *116*, 8693–8749.
- (4) Ash, P. A.; Hidalgo, R.; Vincent, K. A. Proton Transfer in the Catalytic Cycle of [NiFe] Hydrogenases: Insight from Vibrational Spectroscopy. *ACS Catal.* **2017**, *7*, 2471–2485.
- (5) Greene, B. L.; Wu, C.-H.; McTernan, P. M.; Adams, M. W. W.; Dyer, R. B. Proton-Coupled Electron Transfer Dynamics in the Catalytic Mechanism of a [NiFe]-Hydrogenase. *J. Am. Chem. Soc.* **2015**, *137*, 4558–4566.
- (6) Weber, K.; Krämer, T.; Shafaat, H. S.; Weyhermüller, T.; Bill, E.; van Gestel, M.; Neese, F.; Lubitz, W. A Functional [NiFe]-Hydrogenase Model Compound that Undergoes Biologically Relevant Reversible Thiolate Protonation. *J. Am. Chem. Soc.* **2012**, *134*, 20745–20755.
- (7) Ohki, Y.; Yasumura, K.; Ando, M.; Shimokata, S.; Tatsumi, K. A Model for the CO-Inhibited Form of [NiFe] Hydrogenase: Synthesis of $(\text{CO})_3\text{Fe}(\mu\text{-StBu})_3\text{Ni}\{\text{SC}_6\text{H}_5\}_2$, 6-(mesityl) $\}_2$ and Reversible CO Addition at the Ni Site. *Proc. Natl. Acad. Sci. U. S. A.* **2010**, *107*, 3994–3997.
- (8) Ulloa, O. A.; Huynh, M. T.; Richers, C. P.; Bertke, J. A.; Nilges, M. J.; Hammes-Schiffer, S.; Rauchfuss, T. B. Mechanism of H_2 Production by Models for the [NiFe]-Hydrogenases: Role of Reduced Hydrides. *J. Am. Chem. Soc.* **2016**, *138*, 9234–9245.
- (9) Barton, B. E.; Rauchfuss, T. B. Hydride-Containing Models for the Active Site of the Nickel-Iron Hydrogenases. *J. Am. Chem. Soc.* **2010**, *132*, 14877–14885.
- (10) Carroll, M. E.; Barton, B. E.; Gray, D. L.; Mack, A. E.; Rauchfuss, T. B. Active-Site Models for the Nickel-Iron Hydrogenases: Effects of Ligands on Reactivity and Catalytic Properties. *Inorg. Chem.* **2011**, *50*, 9554–9563.
- (11) Ogo, S.; Ichikawa, K.; Kishima, T.; Matsumoto, T.; Nakai, H.; Kusaka, K.; Ohhara, T. A Functional [NiFe]Hydrogenase Mimic That Catalyzes Electron and Hydride Transfer from H_2 . *Science* **2013**, *339*, 682–684.
- (12) Isegawa, M.; Sharma, A. K.; Ogo, S.; Morokuma, K. DFT Study on Fe(IV)-Peroxo Formation and H Atom Transfer Triggered O_2 Activation by NiFe Complex. *Organometallics* **2018**, *37*, 1534–1545.
- (13) Ogata, H.; Nishikawa, K.; Lubitz, W. Hydrogens detected by subatomic resolution protein crystallography in a [NiFe] hydrogenase. *Nature* **2015**, *520*, 571–574.
- (14) Franolic, J. D.; Wang, W. Y.; Millar, M. Synthesis, structure, and characterization of a mixed-valence [nickel(II)nickel(III)] thiolate dimer. *J. Am. Chem. Soc.* **1992**, *114*, 6587–6588.
- (15) Subramanian, R.; Koch, S. A.; Harbison, G. S. Nitrogen-14 NMR and X-ray Crystal Structures of a Series of $[\text{M}^{\text{II}}(\text{SR})_4]^{2-}$ Complexes (M = Manganese, Iron, Cobalt, Nickel, Zinc, Cadmium and Mercury) with S_4 Crystallographic Symmetry. *J. Phys. Chem.* **1993**, *97*, 8625–8629.
- (16) Chen, C.-H.; Lee, G.-H.; Liaw, W.-F. Mononuclear $[\text{Ni}^{\text{II}}(\text{L})(\text{P}(\text{o}-\text{C}_6\text{H}_4\text{S})_2(\text{o}-\text{C}_6\text{H}_4\text{SH}))]^{0/1-}$ (L = Thiolate, Selenolate, PPh₃, and Cl) Complexes with Intramolecular $[\text{Ni}\cdots\text{S}\cdots\text{H}\cdots\text{S}]/[\text{Ni}\cdots\text{H}\cdots\text{S}]$ Interactions Modulated by the Coordinated Ligand L: Relevance to the [NiFe] Hydrogenases. *Inorg. Chem.* **2006**, *45*, 2307–2316.
- (17) Lee, C.-M.; Chuang, Y.-L.; Chiang, C.-Y.; Lee, G.-H.; Liaw, W.-F. Mononuclear Ni(III) Complexes $[\text{Ni}^{\text{III}}(\text{L})(\text{P}(\text{C}_6\text{H}_5)_3\text{-SiMe}_2\text{-S})_3]^{0/1-}$ (L = Thiolate, Selenolate, CH_2CN , Cl, PPh₃): Relevance to the Nickel Site of [NiFe] Hydrogenases. *Inorg. Chem.* **2006**, *45*, 10895–10904.
- (18) Lee, C.-M.; Chiou, T.-W.; Chen, H.-H.; Chiang, C.-Y.; Kuo, T.-S.; Liaw, W.-F. Mononuclear Ni(II)-Thiolate Complexes with Pendant Thiol and Dinuclear Ni(III/II)-Thiolate Complexes with Ni–Ni Interaction Regulated by the Oxidation Levels of Nickels and the Coordinated Ligands. *Inorg. Chem.* **2007**, *46*, 8913–8923.

- (19) Chiou, T.-W.; Liaw, W.-F. Mononuclear Nickel(III) Complexes $[\text{Ni}^{\text{III}}(\text{OR})(\text{P}(\text{C}_6\text{H}_3\text{-}3\text{-SiMe}_3\text{-}2\text{-S})_3)]^-$ (R = Me, Ph) Containing the Terminal Alkoxide Ligand: Relevance to the Nickel Site of Oxidized-Form $[\text{NiFe}]$ Hydrogenases. *Inorg. Chem.* **2008**, *47*, 7908–7913.
- (20) Nguyen, D. H.; Hsu, H.-F.; Millar, M.; Koch, S. A.; Achim, C.; Bominaar, E.; Münck, E. Nickel(II) Thiolate Complex with Carbon Monoxide and Its Fe(II) Analog: Synthetic Models for CO Adducts of Nickel-Iron-Containing Enzymes. *J. Am. Chem. Soc.* **1996**, *118*, 8963–8964.
- (21) Hsu, H.-F.; Koch, S. A.; Popescu, C. V.; Münck, E. Chemistry of Iron Thiolate Complexes with CN^- and CO. Models for the $[\text{Fe}(\text{CO})(\text{CN})_2]$ Structural Unit in Ni-Fe Hydrogenase Enzymes. *J. Am. Chem. Soc.* **1997**, *119*, 8371–8372.
- (22) Motekaitis, R. J.; Martell, A. E.; Koch, S. A.; Hwang, J.-W.; Quarless, D. A.; Welch, M. J. The Gallium(III) and Indium(III) Complexes of Tris(2-mercaptobenzyl)amine and Tris(2-hydroxybenzyl)amine. *Inorg. Chem.* **1998**, *37*, 5902–5911.
- (23) Govindaswamy, N.; Quarless, D. A.; Koch, S. A. New Amine Trithiolate Tripod Ligand and Its Iron(II) and Iron(III) Complexes. *J. Am. Chem. Soc.* **1995**, *117*, 8468–8469.
- (24) Conradie, J.; Quarless, D. A.; Hsu, H.-F.; Harrop, T. C.; Lippard, S. J.; Koch, S. A.; Ghosh, A. Electronic Structure and FeNO Conformation of Nonheme Iron-Thiolate-NO Complexes: An Experimental and DFT Study. *J. Am. Chem. Soc.* **2007**, *129*, 10446–10456.
- (25) Gjoka, B.; Romano, F.; Zonta, C.; Licini, G. Effective Synthesis of ortho-Substituted Trithiophenol Amines by Miyazaki-Newman-Kwart Rearrangement. *Eur. J. Org. Chem.* **2011**, *2011*, 5636–5640 S5636/S631-S5636/S610 .
- (26) Chen, Q.; Buss, C. E.; Young, V. G.; Fox, S. Synthesis and structural Studies of Tris-2-chlorobenzylamine and Tris-2-bromobenzylamine. *J. Chem. Crystallogr.* **2005**, *35*, 177–181.
- (27) Ohki, Y.; Tatsumi, K. Thiolate-Bridged Iron–Nickel Models for the Active Site of $[\text{NiFe}]$ Hydrogenase. *Eur. J. Inorg. Chem.* **2011**, *2011*, 973–985.
- (28) Dawson, J.; Ghiotto, F.; McMaster, J.; Schroeder, M. Metal Complex of Hydrogenase Active Sites. *RSC Energy Environ. Ser.* **2011**, *5*, 326–386.
- (29) Yang, D.; Li, Y.; Su, L.; Wang, B.; Qu, J. Versatile Reactivity of CH_3CN -Coordinated Nickel-Iron Heterodimetallate Complexes with Cp^* Ligand on Diazadithiolate (N_2S_2) or Dithiadithiolate (S_4) Platforms. *Eur. J. Inorg. Chem.* **2015**, *2015*, 2965–2973.
- (30) Canaguier, S.; Field, M.; Oudart, Y.; Pécaut, J.; Fontecave, M.; Artero, V. A Structural and Functional Mimic of the Active Site of NiFe Hydrogenases. *Chem. Commun.* **2010**, *46*, 5876–5878.
- (31) Chu, X.; Yu, X.; Rajee, S.; Angamuthu, R.; Ma, J.; Tung, C.-H.; Wang, W. Synthetic $[\text{NiFe}]$ Models with a Fluxional CO Ligand. *Dalton Trans.* **2017**, *46*, 13681–13685.
- (32) Denny, J. A.; Darenbourg, M. Y. Metallothiolates as Ligands in Coordination, Bioinorganic, and Organometallic Chemistry. *Chem. Rev.* **2015**, *115*, 5248–5273.
- (33) Ichikawa, K.; Matsumoto, T.; Ogo, S. Critical aspects of $[\text{NiFe}]$ hydrogenase ligand composition. *Dalton Trans.* **2009**, 4304–4309.
- (34) Zhu, W.; Marr, A. C.; Wang, Q.; Neese, F.; Spencer, D. J. E.; Blake, A. J.; Cooke, P. A.; Wilson, C.; Schröder, M. Modulation of the Electronic Structure and the Ni-Fe Distance in Heterobimetallic Models for the Active Site in $[\text{NiFe}]$ Hydrogenase. *Proc. Natl. Acad. Sci. U. S. A.* **2005**, *102*, 18280–18285.
- (35) Schmidt, T.; Baumann, W.; Drexler, H. J.; Heller, D. Unusual deactivation in the asymmetric hydrogenation of itaconic acid. *J. Organomet. Chem.* **2011**, *696*, 1760–1767.
- (36) Song, L.-C.; Gao, X.-Y.; Liu, W.-B.; Zhang, H.-T.; Cao, M. Synthesis, Characterization, and Reactions of Functionalized Nickel–Iron Dithiolates Related to the Active Site of $[\text{NiFe}]$ -Hydrogenases. *Organometallics* **2018**, *37*, 1050–1061.
- (37) Speiser, F.; Braunstein, P.; Saussine, L. Catalytic Ethylene Dimerization and Oligomerization: Recent Developments with Nickel Complexes Containing P,N-Chelating Ligands. *Acc. Chem. Res.* **2005**, *38*, 784–793.
- (38) Chu, W.-Y.; Richers, C. P.; Kahle, E. R.; Rauchfuss, T. B.; Arrigoni, F.; Zampella, G. Imine-Centered Reactions in Imino-Phosphine Complexes of Iron Carbonyls. *Organometallics* **2016**, *35*, 2782–2792.
- (39) Kermagoret, A.; Braunstein, P. Mono- and Dinuclear Nickel Complexes with Phosphino-, Phosphinito-, and Phosphonitopyridine Ligands: Synthesis, Structures, and Catalytic Oligomerization of Ethylene. *Organometallics* **2008**, *27*, 88–99.
- (40) Speiser, F.; Braunstein, P.; Saussine, L.; Welter, R. Nickel Complexes with New Bidentate P,N Phosphinitooxazoline and -Pyridine Ligands: Application for the Catalytic Oligomerization of Ethylene. *Inorg. Chem.* **2004**, *43*, 1649–1658.
- (41) Sun, W.-H.; Li, Z.; Hu, H.; Wu, B.; Yang, H.; Zhu, N.; Leng, X.; Wang, H. Synthesis and Characterization of Novel Nickel(II) Complexes Bearing N,P Ligands and their Catalytic Activity in Ethylene Oligomerization. *New J. Chem.* **2002**, *26*, 1474–1478.
- (42) Addison, A. W.; Rao, T. N.; Reedijk, J.; van Rijn, J.; Verschoor, G. C. Synthesis, structure, and spectroscopic properties of copper(II) compounds containing nitrogen-sulphur donor ligands; the crystal and molecular structure of aqua[1,7-bis(N-methylbenzimidazol-2[prime or minute]-yl)-2,6-dithiaheptane]copper(II) perchlorate. *J. Chem. Soc., Dalton Trans.* **1984**, 1349–1356.
- (43) Barton, B. E.; Whaley, C. M.; Rauchfuss, T. B.; Gray, D. L. Nickel-Iron-Dithiolato-Hydrides Relevant to the $[\text{NiFe}]$ -Hydrogenase Active Site. *J. Am. Chem. Soc.* **2009**, *131*, 6942–6943.
- (44) Osakada, K.; Hayashi, H.; Maeda, M.; Yamamoto, T.; Yamamoto, A. Preparation and Properties of new Thiolato- and Mercapto-Transition Metal Complexes, $\text{MR}(\text{SR})(\text{PR}^{\prime}3)_2$ (M = Ni, Pd; R = H, Ar; R' = H, Ar). Evolution of R-R' from the complexes Through Cleavage of the S-R' Bond. *Chem. Lett.* **1986**, *15*, 597–600.
- (45) Tucci, G. C.; Holm, R. H. Nickel-Mediated Formation of Thioesters from Bound Methyl, Thiols, and Carbon Monoxide - a Possible Reaction Pathway of Acetyl-Coenzyme A Synthase Activity in Nickel-Containing Carbon Monoxide Dehydrogenases. *J. Am. Chem. Soc.* **1995**, *117*, 6489–6496.
- (46) Magano, J.; Monfette, S. Development of an Air-Stable, Broadly Applicable Nickel Source for Nickel-Catalyzed Cross-Coupling. *ACS Catal.* **2015**, *5*, 3120–3123.
- (47) Shields, J. D.; Gray, E. E.; Doyle, A. G. A Modular, Air-Stable Nickel Precatalyst. *Org. Lett.* **2015**, *17*, 2166–2169.
- (48) Pal, S.; Ohki, Y.; Yoshikawa, T.; Kuge, K.; Tatsumi, K. Dithiolate-Bridged Fe-Ni-Fe Trinuclear Complexes Consisting of $\text{Fe}(\text{CO})_3(\text{CN})_n$ (n = 0, 1) Components Relevant to the Active Site of $[\text{NiFe}]$ Hydrogenase. *Chem. - Asian J.* **2009**, *4*, 961–968.
- (49) Huynh, M. T.; Schilter, D.; Hammes-Schiffer, S.; Rauchfuss, T. B. Protonation of Nickel–Iron Hydrogenase Models Proceeds after Isomerization at Nickel. *J. Am. Chem. Soc.* **2014**, *136*, 12385–12395.
- (50) Arcas, A.; Royo, P. Bispentafluorophenyl Nickel(II) Complexes. *Inorg. Chim. Acta* **1978**, *30*, 205–207.
- (51) Swenson, D.; Baenziger, N. C.; Coucouvanis, D. Tetrahedral Mercaptide Complexes. Crystal and Molecular Structures of $[(\text{C}_6\text{H}_5)_4\text{P}]_2\text{M}(\text{SC}_6\text{H}_5)_4$ Complexes (M = Cadmium(II), Zinc(II), Nickel(II), Cobalt(II), and Manganese(II)). *J. Am. Chem. Soc.* **1978**, *100*, 1932–1934.
- (52) Krebs, B.; Henkel, G. Transition-Metal Thiolates: From Molecular Fragments of Sulfidic Solids to Models for Active Centers in Biomolecules. *Angew. Chem., Int. Ed. Engl.* **1991**, *30*, 769–788.
- (53) Block, E.; Ofori-Okai, G.; Zubieta, J. 2-Phosphino- and 2-phosphinylbenzenethiols: new ligand types. *J. Am. Chem. Soc.* **1989**, *111*, 2327–2329.
- (54) Govindaswamy, K. Synthesis and Characterization of Novel Polydentate Ligands and Transition Metal Chalcogenides. Ph.D. Thesis, State University of New York at Stony Brook, 1995.
- (55) Quarless, D. A., Jr. The Synthesis and Characterization of Complexes of Novel Tetradentate Thio Amine Ligand. Ph.D. Thesis, State University of New York, Stony Brook, 1997.

- (56) Crochet, P.; Gimeno, J.; Borge, J.; García-Granda, S. Novel Ruthenium(II) Complexes Containing Imino- or Aminophosphine Ligands for Catalytic Transfer Hydrogenation. *New J. Chem.* **2003**, *27*, 414–420.
- (57) Catheline, D.; Astruc, D. Piano-Stool (Pentamethylcyclopentadienyl)iron Complexes: Syntheses and Simple Coordination Chemistry. *Organometallics* **1984**, *3*, 1094–1100.
- (58) Brazzolotto, D.; Gennari, M.; Queyriaux, N.; Simmons, T. R.; Pécaut, J.; Demeshko, S.; Meyer, F.; Orio, M.; Artero, V.; Duboc, C. Nickel-Centred Proton Reduction Catalysis in a Model of [NiFe] Hydrogenase. *Nat. Chem.* **2016**, *8*, 1054–1060.
- (59) Ward, L. G. L. Anhydrous Nickel(II) Halides and Their Tetrakis(ethanol) and 1,2-Dimethoxyethane Complexes. *Inorg. Syn.* **1971**, *13*, 154–164.
- (60) Manuel, T. A. Some Tertiary Phosphine-Iron Carbonyl Compounds. *Inorg. Chem.* **1963**, *2*, 854–858.
- (61) Hieber, W.; Bader, G. Über Metallcarbonyle. VI. Neuartige Kohlenoxydverbindungen von Eisenhalogeniden und ihre chemische Charakterisierung. *Z. anorg. allgem. Chem.* **1930**, *190*, 193–214.
- (62) Carroll, M. E.; Chen, J.; Gray, D. E.; Lansing, J. C.; Rauchfuss, T. B.; Schilter, D.; Volkers, P. I.; Wilson, S. R. Ferrous Carbonyl Dithiolates as Precursors to FeFe, FeCo, and FeMn Carbonyl Dithiolates. *Organometallics* **2014**, *33*, 858–867.
- (63) Zhou, X.; Barton, B. E.; Chambers, G. M.; Rauchfuss, T. B.; Arrigoni, F.; Zampella, G. Preparation and Protonation of Fe₂(pdt)-(CNR)₆, Electron-Rich Analogues of Fe₂(pdt)(CO)₆. *Inorg. Chem.* **2016**, *55*, 3401–3412.
- (64) SAINT, SHELXTL, XCIF, XPREP; Bruker AXS, Inc.: Madison, WI, 2014.
- (65) Krause, L.; Herbst-Irmer, R.; Sheldrick, G. M.; Stalke, D. Comparison of Silver and Molybdenum Microfocus X-Ray Sources for Single-Crystal Structure Determination. *J. Appl. Crystallogr.* **2015**, *48*, 3–10.
- (66) Sheldrick, G. M. SHELXT - Integrated Space-Group and Crystal-Structure Determination. *Acta Crystallogr., Sect. A: Found. Adv.* **2015**, *A71*, 3–8.
- (67) Schäfer, A.; Huber, C.; Ahlrichs, R. Fully Optimized Contracted Gaussian Basis Sets of Triple Zeta Valence Quality for Atoms Li to Kr. *J. Chem. Phys.* **1994**, *100*, 5829–5835.
- (68) Grimme, S. Semiempirical GGA-Type Density Functional Constructed with a Long-Range Dispersion Correction. *J. Comput. Chem.* **2006**, *27*, 1787–1799.
- (69) Furche, F.; Ahlrichs, R.; Hättig, C.; Klopper, W.; Sierka, M.; Weigend, F. Turbomole. *Wiley Interdisc. Rev.: Comput. Mol. Sci.* **2014**, *4*, 91–100.
- (70) Li, Q.; Lalaoui, N.; Woods, T. J.; Rauchfuss, T. B.; Arrigoni, F.; Zampella, G. Electron-Rich, Diiron Bis(monothiolato) Carbonyls: C-S Bond Homolysis in a Mixed Valence Diiron Dithiolate. *Inorg. Chem.* **2018**, *57*, 4409–4418.
- (71) Eichkorn, K.; Weigend, F.; Treutler, O.; Ahlrichs, R. Auxiliary Basis Sets for Main Row Atoms and Transition Metals and Their Use to Approximate Coulomb Potentials. *Theor. Chem. Acc.* **1997**, *97*, 119–124.
- (72) Noodleman, L.; Case, D. A.; Aizman, A. Broken symmetry analysis of spin coupling in iron-sulfur clusters. *J. Am. Chem. Soc.* **1988**, *110*, 1001–1005.
- (73) Ditchfield, R. Self-Consistent Perturbation Theory of Diamagnetism I. A Gauge-Invariant LCAO Method for N.M.R. Chemical Shifts. *Mol. Phys.* **1974**, *27*, 789–807.
- (74) Wolinski, K.; Hinton, J. F.; Pulay, P. Efficient implementation of the gauge-independent atomic orbital method for NMR chemical shift calculations. *J. Am. Chem. Soc.* **1990**, *112*, 8251–8260.
- (75) Arrigoni, F.; Bertini, L.; De Gioia, L.; Cingolani, A.; Mazzoni, R.; Zanotti, V.; Zampella, G. Mechanistic Insight into Electrocatalytic H₂ Production by [Fe₂(CN){μ-CN(Me)₂}(μ-CO)(CO)(Cp)₂]: Effects of Dithiolate Replacement in [FeFe] Hydrogenase Models. *Inorg. Chem.* **2017**, *56*, 13852–13864.
- (76) Siegbahn, P. E. M.; Tye, J. W.; Hall, M. B. Computational Studies of [NiFe] and [FeFe] Hydrogenases. *Chem. Rev.* **2007**, *107*, 4414–4435.